Geol. Mag. **145** (*1*), *2008, pp. 37–54. © 2007 Cambridge University Press*
doi:10.1017/S0016756807003986 First published online 30 November 2007 *Printed in the United Kingdom*

Geochemical characteristics of mafic lavas from the Neotethyan ophiolites in western Turkey: implications for heterogeneous source contribution during variable stages of ocean crust generation

E. ALDANMAZ*§, M. K. YALINIZ†, A. GÜCTEKIN* & M. C. GÖNCÜOĞLU‡

*Department of Geology, University of Kocaeli, Izmit 41040, Turkey
†Department of Civil Engineering, Celal Bayar University, Manisa, Turkey
‡Department of Geology, Middle East Technical University, Ankara 0653, Turkey

(*Received* 18 December 2006; *accepted* 31 May 2007)

Abstract – The Late Triassic to Late Cretaceous age mafic lavas from the Neotethyan suture zone ophiolites in western Turkey exhibit a wide diversity of geochemical signatures, indicating derivation from extremely heterogeneous mantle sources. The rocks as a whole can be divided into three broad subdivisions based on their bulk-rock geochemical characteristics: (1) mid-ocean ridge basalts (MORB) that range in composition from light rare earth element (LREE)-depleted varieties (N-MORB; $(La/Sm)_N < 1$) through transitional MORB to LREE enriched types (E-MORB; $(La/Sm)_N > 1$); (2) the ocean island basalt (OIB)-type alkaline volcanic rocks with significant enrichment in LILE, HFSE and L-MREE, and a slight depletion in HREE, relative to normal mid-ocean ridge basalts (N-MORB); and (3) the supra-subduction zone (SSZ)-type tholeiites originated from arc mantle sources that are characterized by selective enrichments in fluid-soluble large ion lithophile elements (LILE) and LREE relative to the high field strength elements (HFSE). The formation of MORB tholeiites with variable enrichments and depletions in incompatible trace elements is probably related to the processes of crust generation along an oceanic spreading system, and the observed MORB–OIB associations can be modelled by heterogeneous source contribution and mixing of melts from chemically discrete sources from sub-lithospheric reservoirs. Evaluation of trace element systematics shows that the inferred heterogeneities within the mantle source regions are likely to have originated from continuous processes of formation and destruction of enriched mantle domains by long-term plate recycling, convective mixing and melt extraction. The origin of SSZ-type tholeiites with back-arc basin affinities, on the other hand, can be attributed to the later intra-oceanic subduction and plate convergence which led to the generation of supra-subduction-type oceanic crust as a consequence of imparting a certain extent of subduction component into the mantle melting region. Mixing of melts from a multiply depleted mantle source, which subsequently received variable re-enrichment with a subduction component, is suggested to explain the generation of supra-subduction-type oceanic crust. The geodynamic setting in which much of the SSZ-type ophiolitic extrusive rocks from western Turkey were generated can be described as an arc-basin system that is characterized by an oceanic lithosphere generation most probably associated with melting of mantle material along a supra-subduction-type spreading centre.

Keywords: MORB heterogeneity, mid-plate basalts, back-arc basin basalts, Neotethyan ophiolites, western Turkey, mantle heterogeneity.

1. Introduction

Magmatic products from the crustal parts of ophiolite complexes can provide important information on the processes of melt generation during variable stages of lithosphere production, contribute to our understanding of the original tectonic setting for the formation of oceanic lithosphere, and help in understanding the processes of crustal accretion in variable tectonic systems. Geochemical studies of basaltic products from obducted slabs of old oceanic lithospheres are especially important in identifying the structure and magmatic evolution of oceanic crust formed in ancient spreading centres and in interpreting the geological history of regions which comprise various tectonic units of accreted terranes (e.g. accreted units of arc-basin systems: Shervais, 2001; Pearce, 2003).

The geological characteristics of many of the ophiolite fragments across Turkey reflect the evolution of the Late Triassic to Late Cretaceous terranes of the eastern Mediterranean and have long been central to our understanding of the Neotethyan evolution in this region, as well as the Late Cretaceous tectonics of Anatolia (e.g. Şengör & Yılmaz, 1981; Dilek *et al.* 1999; Robertson, 2002). It is commonly accepted that the northern part of the present Anatolian plate (Şengör & Yılmaz, 1981) comprises a number of terranes (Göncüoğlu, Dirik & Kozlu, 1997) or continental

§Author for correspondence: ercan.aldanmaz@dunelm.org.uk

micro-plates that were amalgamated by the closure of the Tethyan oceanic realm mainly by northward-directed subduction events. The İzmir–Ankara suture zone is one of the major geological discontinuities in the region and extends over 1000 km. It represents the scar of the Tethyan oceanic realm between the Gondwanan Tauride–Anatolide microplate in the south and the Sakarya Composite Terrane (Göncüoğlu *et al.* 2000) of disputed origin in the north. This suture zone is marked, in some parts, by an intense high-pressure/low-temperature blueschist-facies metamorphism (Sherlock *et al.* 1999; Okay, 2002) and contains a number of disrupted ophiolite fragments that are interpreted to represent remnants of the Tethyan oceanic lithosphere (Central Anatolia: Yalınız, Floyd & Göncüoğlu, 1996; Gürer & Aldanmaz, 2002; Central Sakarya: Göncüoğlu *et al.* 2000; NW Anatolia: Aldanmaz & Köprübaşı, 2006). The fragments of this oceanic lithosphere were emplaced mostly southward onto the passive margin sequences of the Anatolite–Tauride platform as a result of the Mesozoic accretion of arc-related terranes (e.g. Göncüoğlu, Yalınız & Tekin, 2006*a*).

In this contribution we examine the mafic extrusive rocks from the Late Triassic to Late Cretaceous age oceanic fragments along the western part of the İzmir–Ankara suture zone, and present a new geochemical dataset for the lavas. The data provide a robust tool for investigating the petrogenetic and geodynamic evaluation of this segment of the İzmir–Ankara zone ophiolites, because the province contains accreted units of mafic volcanic rocks, the composition of which can be used to document variable stages of oceanic crust generation during different styles of plate motions, including the early plate divergence, later plate convergence and possibly the latest slab steepening and back-arc opening. We focus particularly on modelling and interpreting bulk-rock trace element data, with a special emphasis on providing insights into: (1) the characteristics of the mantle source of the mafic magma(s) in terms of chemical composition; (2) the primary controls on melt generation and crust production processes; and (3) the identification of possible tectonic setting(s) in which the oceanic lithosphere(s) were generated prior to emplacement.

2. Geological summary

The Late Mesozoic to Early Cenozoic evolution of western Turkey is linked to the closure of the Tethyan ocean, and is largely characterized by plate subduction, ophiolite obduction, high-pressure/low-temperature metamorphism and collision of accreted continental blocks. The ophiolitic lavas within the western part of the İzmir–Ankara suture zone represent remnants of the crustal parts of an oceanic lithosphere, which is interpreted to have formed in an ocean basin, comprised a part of the Tethyan ocean floor (Şengör & Yılmaz, 1981) and, subsequent to the Late Cretaceous (*c*. 90 Ma: Okay, Tansel & Tüysüz, 2001; Önen, 2003) intra-oceanic thrusting, north-dipping subduction and the later collision events, emplaced southward onto the passive margin volcano-sedimentary sequences of the Tauride–Anatolide platform (e.g. Göncüoğlu *et al.* 2000) (Fig. 1a). The Mesozoic to Early Cenozoic history of the collision zone is recorded by sedimentary and volcanic rock associations that have been scraped off the Tethyan seafloor, disrupted and incorporated into the mélange associations to form an ophiolite–flysch range (known as the Bornova Flysch zone: Erdoğan, 1990), and then thrust over the northern edge of the Tauride–Anatolide platform along with ophiolite nappes during Late Cretaceous times.

The Bornova Flysch Zone forms a NNE–SSW-trending belt 50 to 90 km in width and about 200 km in length and consists of chaotically deformed Upper Cretaceous to Lower Paleocene clastic rocks with Mesozoic (Middle Triassic to Cretaceous) neritic limestones, and Late Triassic (Tekin, Göncüoğlu & Turhan, 2002; Tekin *et al.* unpub. TUBITAK rep. no. 103Y027, 2006) to Late Cretaceous (Göncüoğlu, Yalınız & Tekin, 2006*b*) mafic lavas with cherts and pelagic shales as well as blocks of ultramafic rocks (Erdoğan, 1990; Yalınız & Göncüoğlu, unpub. TUBITAK rep. no. 199Y100, 2005). Flysch sediments contain a large amount of limestone blocks derived from a Mesozoic carbonate platform that represented the northwestern margin of the Tauride–Anatolide block. Throughout the suture zone are found isolated outcrops of dismembered ophiolite units containing ultramafic peridotites and/or mafic extrusive rocks (Fig. 1b). The latter consist mainly of basaltic pillowed and massif lava flows.

The lavas from the sampling sites of this study within the Tethyan suture zone in western Turkey constitute three discrete petrological groups based on their bulk-rock geochemical characteristics: (1) mid-ocean ridge basalt (MORB)-type oceanic tholeiites; (2) ocean island basalt (OIB)-type mid-plate alkali basalts; and (3) supra-subduction zone (SSZ)-type tholeiites. In the southwestern part of the Bornova Flysch Zone, around the city of Manisa (Fig. 1b), the dominant rock types are MORB tholeiites that are in close association with large amounts of OIB-type alkaline basaltic lavas. Radiolarian cherts associated with these basaltic lavas, being either inter-pillow sediments or local intercalations of pelagic or hemi-pelagic origin, have yielded similar age determinations for both types of lavas that range from the Middle Jurassic to Lower Cretaceous (Göncüoğlu, Yalınız & Tekin, 2006*b*). Similar ages of sedimentary covers and close associations of these rock groups suggest that both rock groups originated simultaneously in the same oceanic basin and are genetically related.

Further northeast within the Bornova Flysch Zone, to the northeast of Akhisar (Fig. 1b), the tholeiitic lavas with SSZ geochemical affinities become the dominant

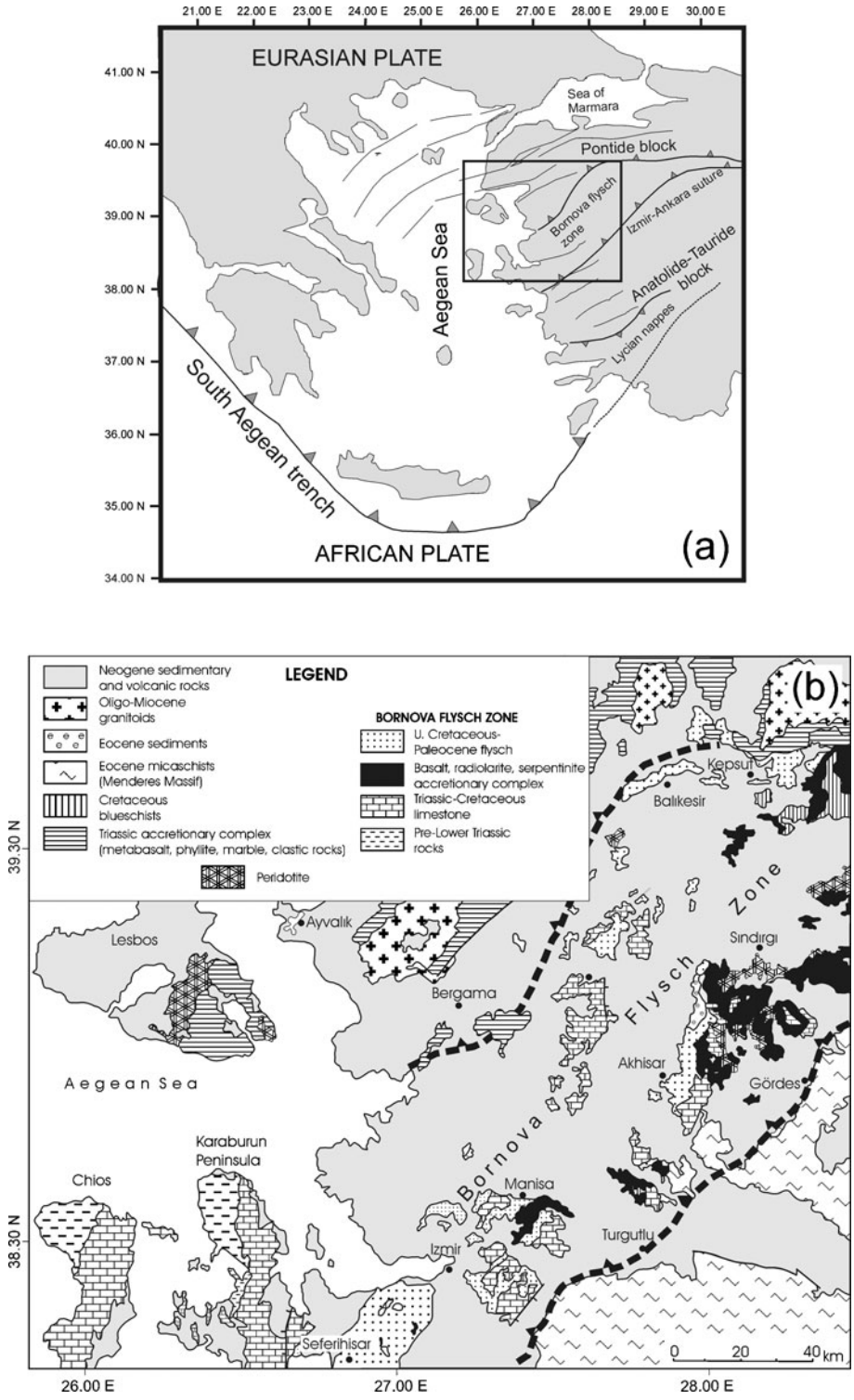

Figure 1. (a) Regional tectonic map showing the major geological features of the Aegean section of the eastern Mediterranean. (b) Simplified geological map showing the distribution of main lithological units within the Tethyan suture zone in western Turkey (based on the data compiled from Erdoğan, 1990; Okay, Tansel & Tüysüz, 2001; Yalınız & Göncüoğlu, unpub. TÜBİTAK rep. no. 199Y100, 2005).

rock types. In this part, the ophiolitic suite contains mafic lavas that range in composition from depleted MORB with a slight subduction signature to those with clear enrichment in subduction components. Both depleted and subduction-enriched lavas alternate with each other, suggesting that they are indistinguishable in their origin and were probably formed along the same spreading centre. Radiolarian cherts associated with these SSZ-type lavas have yielded ages between late Early Cretaceous and Late Cretaceous (Cenomanian)

(Göncüoğlu, Yalınız & Tekin, 2006*b*). These ages are comparable to those obtained from SSZ-type ophiolitic lavas from other parts of the İzmir–Ankara suture zone (e.g. Göncüoğlu, Yalınız & Tekin, 2006*a*) and provide constraints on the formation age of SSZ-type oceanic lithosphere during the evolution of the Tethyan ocean in this part of the eastern Mediterranean.

3. Sample description

Oceanic tholeiites are the most abundant rock types within the suites and comprise both MORB- and SSZ-type tholeiitic rock associations. The two groups are petrographically indistinguishable regardless of their petrological type and age. They crop out as black to reddish-brown pillows and massive flows. The basalts are predominantly aphyric or microporphyritic with equigranular to intergranular groundmass consisting of plagioclase, clinopyroxene, titanium-rich magnetite and ilmenite. The average modal abundances of the constituting mineral phases are estimated to be 55 % plagioclase, 35 % clinopyroxene, 6 % titanium-rich magnetite, 3–5 % olivine, and 2–3 % ilmenite. Secondary mineral replacements within the crystals are common along the margins of the grains or along the twin planes. A majority of the samples contain euhedral plagioclase with little or no alteration, but other samples show complete alteration or replacement of plagioclase by albite, Ca-zeolites and prehnite. Clinopyroxene is colourless, granular to sub-ophitic grains of augite. Alteration of pyroxenes is to chlorite, magnetite, epidote and actinolite. Olivine crystals can be identified in a few samples as relict pseudomorphs, partially replaced by chlorite and clay minerals. Oxide phases occur as granular crystals ranging in size from 0.005 to 0.1 mm, found in intergranular spaces between the plagioclase and pyroxene grains.

Alkali basalts are the second most common rock types within the lava suites. The common textures in alkali basalts vary between sub-ophitic, porphyritic and seriate with total phenocryst contents ranging from 10 to 20 %. The lavas generally contain phenocrysts of plagioclase (about 50 %), titanian augite (30 %) and less olivine (15 %) in a fine-grained groundmass containing granular olivine, plagioclase laths and intersertal glass. Other primary phases include ilmenite and titanium-rich magnetite. Some glassy rocks have phenocrysts of equant to elongate-skeletal olivine with included or attached oxide phases in a dark brown glass. Secondary phases include chloride, calcite, epidote and titanite.

4. Bulk-rock chemistry

4.a. Analytical data

Only the best-preserved basaltic rock samples with no signs of alteration were chosen for geochemical analysis. External surfaces of rock samples were removed by splitting the samples into chips, which were then ground to a powder in a tungsten carbide ring grinder. Rock samples were analysed for their whole-rock major oxide and selected trace element concentrations (Rb, Sr, Zr, Y, Nb, Ba, Cr, V, Cu, Ni and Zn) using X-ray fluorescence (XRF) at the ALS Chemex Analytical Laboratories in Toronto, Canada. Major and trace element abundances were measured on fused discs and pressed pellets, respectively. Loss-on-ignition was determined by heating a separate aliquot of rock powder at 900 °C. The samples were additionally analysed at the same laboratory for their REE and other trace element concentrations. Rock powders were first fused to ensure dissolution of all phases and then dissolved in hot HF and HNO_3 to prepare the solutions from which trace element abundances were determined using inductively coupled plasma mass spectrometry (ICP-MS). The analytical uncertainties were estimated to be < 1 (SiO_2, TiO_2, Fe_2O_3, MnO, CaO) to 4 (K_2O) relative per cent for major elements, < 5 (Sr, Zr, Y, Nb, Th, U, Hf, Ta) to 15 (Ni, Zn, Cr) relative per cent for minor and trace elements, and < 4 to 10 relative per cent for REE. Whole-rock major and trace element data for the samples are presented in Table 1 as three separate units, namely the MORB, OIB and SSZ suites.

4.b. Major and trace element variations

Although an attempt has been made to minimize the effect of alteration by screening the samples for primary volcanic features, such as pillow structures, and for absence of secondary mineralization, relatively high loss-on-ignition values (2.3–5.5 wt %) for most of the basaltic rocks imply a possible sea-floor alteration. Thus, we consider it unlikely that the measured mobile element abundances are pristine, and we based our modelling and interpretation largely on immobile HFSE, REE and Th.

The rocks as a whole can be classified as basalt with their silica concentrations ranging from 43.7 to 51.6 SiO_2 wt %, although a few samples from the SSZ tholeiitic suite exhibit slight enrichment in SiO_2 (52.7 wt %). The rocks from all three units show relatively wide ranges of Cr and Ni concentrations (Table 1), suggesting extensive fractional crystallization. Samples from the MORB suite contain intermediate TiO_2 (0.76–1.69 wt %), whereas the SSZ-type tholeiites have relatively low TiO_2 (< 1.10 wt %). Samples with the OIB-type affinities are characterized by significantly higher TiO_2 contents that range from 1.04 to 3.68 wt %. The rocks of this latter group are mostly silica-undersaturated (nepheline-normative) and possess higher MgO content than the rocks of the other two groups at a given silica content.

In a ternary element plot of Zr–Th–Nb, the samples classify as MORB and within-plate OIB, with some samples having relative enrichment in Th present in

Table 1. Whole-rock geochemical data for basaltic lavas from the ophiolite suites of western Turkey

Sample no.	SP49	SP40	SP44	SP22	SP32	TU23	TU21	AK31	AK17	AK19	AK20	SP12	SP15	SP14	SP9	AK1	AK5	SP13	SP1	SP7	SP26
Locality	Manisa	Manisa	Manisa	Manisa	Manisa	Manisa	Manisa	Akhisar	Akhisar	Akhisar	Akhisar	Manisa	Manisa	Manisa	Manisa	Akhisar	Akhisar	Manisa	Manisa	Manisa	Manisa
Rock type	N-MORB	N-MORB	N-MORB	N-MORB	N-MORB	N-MORB	N-MORB	N-MORB	N-MORB	N-MORB	N-MORB	E-MORB	E-MORB	E-MORB	E-MORB	E-MORB	E-MORB	OIB	OIB	OIB	OIB
SiO_2	49.86	50.65	50.81	47.43	50.25	49.25	50.25	50.40	50.75	48.84	50.45	49.50	50.15	47.24	50.25	49.75	50.65	46.47	48.97	47.10	44.45
TiO_2	1.02	0.86	1.00	1.18	1.15	0.84	0.84	0.87	1.15	0.76	1.08	1.09	1.34	1.41	1.04	1.69	1.45	1.04	1.09	1.19	2.55
Al_2O_3	15.41	15.81	15.81	15.84	14.63	16.12	15.17	15.22	15.02	16.82	15.17	16.80	15.02	15.72	16.02	16.72	15.87	13.68	14.07	14.25	14.65
Fe_2O_3	10.22	9.23	9.27	7.20	10.91	9.40	9.23	9.29	10.42	9.28	10.11	8.30	10.21	10.75	9.72	8.86	10.21	9.39	7.87	9.25	11.48
MnO	0.18	0.13	0.13	0.22	0.20	0.17	0.17	0.17	0.18	0.17	0.18	0.14	0.19	0.17	0.18	0.15	0.18	0.11	0.10	0.14	0.14
MgO	7.23	6.56	6.51	8.17	7.14	8.60	8.14	7.81	7.33	8.65	7.51	7.67	6.64	7.87	7.26	6.42	6.87	9.21	8.11	9.51	8.94
CaO	9.24	9.12	8.88	10.16	8.47	8.96	9.45	9.45	8.86	9.17	9.09	10.95	8.20	8.54	8.93	9.07	8.54	11.12	10.35	8.88	9.18
Na_2O	3.36	3.97	3.08	3.46	2.69	2.17	2.09	2.06	2.40	2.11	2.27	2.72	3.05	3.01	2.57	2.96	2.43	4.08	4.24	4.16	3.94
K_2O	0.06	0.08	0.09	0.09	0.13	0.04	0.05	0.05	0.16	0.04	0.10	0.11	0.33	0.34	0.17	0.81	0.22	0.83	0.86	0.76	1.31
P_2O_5	0.09	0.07	0.09	0.10	0.13	0.08	0.07	0.08	0.12	0.07	0.11	0.12	0.23	0.28	0.12	0.29	0.16	0.24	0.27	0.26	0.75
LOI	2.80	3.51	4.11	5.18	4.17	3.97	3.86	3.64	3.25	3.26	3.91	2.31	3.78	4.43	3.01	3.27	2.94	3.52	3.72	3.87	2.34
Total	99.47	99.99	99.78	99.03	99.87	99.59	99.34	99.03	99.64	99.16	99.97	99.71	99.15	99.75	99.27	99.98	99.52	99.69	99.65	99.37	99.73
Sc	44.2	39.0	37.6	38.8	44.1	42.1	44.3	47.3	49.4	43.5	46.0	31.4	41.5	36.9	41.2	39.5	42.5	4.9	4.9	5.5	3.0
Cr	143.6	163.5	183.3	203.2	123.7	418.4	428.4	364.6	184.9	357.2	374.2	93.7	102.2	260.2	220.4	280.3	304.9	244.2	277.9	311.7	345.4
V	245.3	232.7	220.2	267.6	252.0	215.4	187.1	192.1	293.8	175.9	211.3	256.7	287.3	276.6	237.8	320.3	271.0	188.1	163.7	184.3	308.2
Ni	68.5	72.0	75.5	79.0	63.3	142.5	100.4	86.9	74.5	135.8	89.2	74.1	53.8	91.7	74.2	114.1	92.0	126.5	285.0	200.9	173.8
Co	58.6	57.0	55.4	53.9	53.8	47.3	46.4	42.2	44.5	43.0	40.1	50.8	49.7	45.4	49.7	48.9	37.8	57.5	53.5	69.5	65.4
Cu	89.1	89.2	89.2	89.3	88.4	95.4	86.2	87.7	82.7	108.0	78.4	44.8	80.7	76.7	83.2	75.9	72.4	47.9	44.6	57.9	54.5
Zn	80.9	79.5	78.0	76.5	79.9	62.2	63.6	63.7	68.9	56.0	71.7	54.5	85.1	64.4	86.7	73.4	76.6	74.7	73.4	72.1	70.8
Ga	16.9	16.7	16.4	16.2	16.8	13.9	13.9	14.2	15.7	13.4	15.0	15.2	17.9	15.7	16.6	17.4	16.2	14.3	17.4	15.5	18.7
Rb	6.8	5.2	4.7	2.6	3.3	1.7	1.0	1.1	2.9	0.6	1.8	2.6	5.7	7.6	3.9	7.6	5.1	21.1	23.2	18.1	14.8
Sr	189.9	83.2	75.5	200.1	125.2	99.2	74.2	75.0	101.1	86.9	87.5	86.1	209.6	291.0	129.9	323.9	111.2	170.7	423.3	350.0	141.7
Y	22.32	18.20	18.80	21.40	24.79	18.47	19.61	18.25	22.81	17.06	22.63	25.21	25.66	21.63	22.88	24.15	30.66	17.83	19.37	22.65	29.38
Zr	51.42	57.49	64.08	61.33	63.61	44.49	51.86	45.06	73.39	40.31	57.53	67.77	102.18	118.13	66.33	135.51	79.39	135.56	135.18	139.96	245.08
Nb	1.87	2.41	1.96	2.51	3.61	1.25	1.55	1.69	3.11	1.13	2.46	3.11	11.75	16.68	4.09	18.09	6.17	25.76	27.71	22.76	65.06
Cs	0.30	0.08	1.50	0.60	0.05	0.10	0.01	0.01	0.07	0.01	0.03	0.03	0.13	0.19	0.08	0.24	0.08	0.83	0.62	0.70	0.30
Ba	66.03	30.02	26.01	27.04	31.54	16.40	9.50	11.19	24.22	6.38	20.48	22.36	91.85	178.82	39.00	222.01	55.57	221.30	243.00	197.00	234.30
La	2.32	1.99	2.42	2.94	3.61	1.40	1.49	1.65	3.16	1.28	2.58	3.31	9.45	11.67	3.75	12.01	6.29	14.11	15.34	14.11	42.14
Ce	6.73	5.52	6.89	8.28	9.29	4.21	4.68	4.89	8.83	4.22	7.64	9.32	19.21	24.55	10.01	26.05	14.19	28.71	32.78	28.36	90.89
Pr	1.12	0.87	1.12	1.30	1.43	0.75	0.78	0.85	1.35	0.72	1.21	1.41	2.42	3.30	1.32	3.45	2.11	3.54	3.81	3.67	10.53
Nd	5.83	4.83	5.83	6.77	7.25	4.52	4.42	4.58	7.02	3.96	6.19	7.55	11.13	13.51	6.53	15.05	9.71	15.01	16.31	16.12	43.22
Sm	2.01	1.65	1.97	2.26	2.33	1.61	1.62	1.65	2.25	1.44	2.22	2.34	3.11	3.41	2.17	3.58	3.05	3.18	3.46	3.58	8.67
Eu	0.75	0.63	0.74	0.85	0.87	0.61	0.62	0.67	0.85	0.54	0.84	0.90	1.19	1.07	0.79	1.14	1.11	0.97	1.10	1.09	2.64
Gd	2.76	2.26	2.67	3.01	3.09	2.25	2.29	2.31	3.10	2.09	3.02	3.11	3.54	3.44	2.84	3.71	3.92	2.75	3.33	3.25	7.59
Tb	0.49	0.45	0.47	0.57	0.59	0.40	0.45	0.42	0.53	0.41	0.53	0.63	0.67	0.60	0.55	0.67	0.68	0.41	0.46	0.58	1.03
Dy	3.41	2.89	3.41	3.71	3.92	2.81	2.89	2.91	3.69	2.65	3.74	4.04	4.01	3.76	3.57	4.01	4.71	2.32	2.61	3.13	4.97
Ho	0.77	0.65	0.77	0.84	0.87	0.64	0.66	0.67	0.82	0.59	0.84	0.93	0.89	0.79	0.79	0.88	1.04	0.46	0.55	0.63	1.02
Er	2.19	1.88	2.21	2.39	2.44	1.88	1.89	1.92	2.31	1.76	2.37	2.65	2.49	2.21	2.25	2.39	2.89	1.43	1.57	1.98	2.69
Tm	0.33	0.29	0.34	0.36	0.37	0.29	0.28	0.28	0.34	0.26	0.34	0.40	0.36	0.32	0.33	0.34	0.43	0.21	0.24	0.29	0.39
Yb	2.11	1.85	2.31	2.35	2.47	1.89	1.81	1.88	2.28	1.75	2.28	2.71	2.40	2.16	2.22	2.28	2.80	1.28	1.40	1.81	2.38
Lu	0.31	0.28	0.35	0.36	0.36	0.28	0.28	0.26	0.34	0.27	0.33	0.43	0.34	0.34	0.31	0.34	0.44	0.19	0.22	0.27	0.35
Hf	1.43	1.25	1.41	1.65	1.71	1.15	1.18	1.19	1.71	1.09	1.57	1.75	2.21	2.64	1.61	2.75	2.09	2.44	2.96	3.05	6.48
Ta	0.11	0.13	0.08	0.15	0.24	0.08	0.09	0.11	0.20	0.07	0.15	0.17	0.49	0.92	0.22	1.13	0.34	1.65	1.59	1.48	3.14
Pb	0.51	0.47	0.43	0.39	0.34	0.01	0.05	0.08	0.16	0.04	0.16	0.11	0.55	0.72	0.76	0.73	0.36	2.56	1.34	2.78	5.71
Th	0.13	0.14	0.13	0.16	0.23	0.11	0.09	0.14	0.30	0.08	0.17	0.23	0.65	0.82	0.30	1.16	0.45	1.83	1.85	1.95	4.85
U	0.05	0.07	0.07	0.06	0.09	0.03	0.04	0.04	0.09	0.03	0.08	0.09	0.36	0.31	0.11	0.65	0.18	1.10	0.91	0.90	1.30

Table 1. (continued)

Sample no.	SP27	AK23	SP83	TU8	TU3	TY4	TU28	AK14	SP28	SP19	SP16	SP20	SP46	SP48	SP37	TU11	TU13	AK8	AK18	AK22	AK26
Locality	Manisa	Manisa	Manisa	Manisa	Manisa	Manisa	Manisa	Akhisar	Akhisar	Manisa	Manisa	Manisa	Manisa	Manisa	Manisa	Manisa	Manisa	Manisa	Akhisar	Akhisar	Akhisar
Rock type	OIB	OIB	OIB	OIB	OIB	OIB	OIB	OIB	OIB	SSZ	SSZ	SSZ	SSZ	SSZ	SSZ	SSZ	SSZ	SSZ	SSZ	SSZ	SSZ
SiO_2	45.29	44.14	43.70	44.62	46.40	46.23	45.83	45.98	45.66	51.22	50.79	47.17	48.51	52.75	47.92	50.01	47.25	50.55	51.51	50.33	47.25
TiO_2	2.67	2.88	3.68	3.11	1.75	1.12	1.13	1.74	2.19	0.90	0.90	0.98	0.90	1.07	0.91	0.99	0.96	0.74	0.58	1.01	0.94
Al_2O_3	12.88	12.37	13.40	12.12	12.55	10.74	12.59	13.71	12.20	14.61	13.21	13.86	14.05	14.40	16.47	14.81	14.45	16.77	14.91	15.44	13.96
Fe_2O_3	10.35	11.56	9.55	9.91	10.33	11.02	10.47	11.01	11.20	10.53	10.25	10.53	9.79	9.27	11.14	9.27	10.16	9.58	9.89	8.70	10.46
MnO	0.12	0.14	0.12	0.11	0.12	0.12	0.12	0.12	0.12	0.16	0.19	0.15	0.15	0.17	0.18	0.15	0.16	0.16	0.15	0.19	0.17
MgO	8.60	9.38	8.18	7.64	9.96	12.69	9.28	8.94	8.77	6.01	7.92	7.79	5.18	5.78	7.17	6.35	6.48	5.67	5.96	6.47	6.48
CaO	11.54	11.36	10.85	11.45	9.84	9.54	10.71	9.88	9.17	8.87	9.98	10.62	11.39	10.03	8.95	8.73	10.98	8.38	9.16	8.32	11.01
Na_2O	2.58	3.71	4.41	4.76	3.59	2.40	3.79	4.11	3.79	2.95	2.64	2.73	3.76	3.47	3.10	3.21	3.25	3.48	2.80	3.29	3.25
K_2O	1.23	1.24	1.73	1.99	0.71	0.58	1.01	1.17	1.62	0.18	0.19	0.22	0.30	0.24	0.21	0.18	0.19	0.14	0.06	0.19	0.15
P_2O_5	0.75	0.76	1.16	0.99	0.36	0.24	0.28	0.42	0.63	0.11	0.09	0.12	0.11	0.14	0.11	0.11	0.09	0.08	0.06	0.14	0.11
LOI	3.40	2.25	3.12	3.16	4.70	3.70	4.56	3.15	3.23	4.40	3.34	5.10	5.49	2.50	3.72	5.46	5.15	3.80	4.55	5.25	5.35
Total	99.41	99.79	99.90	99.86	100.31	98.38	99.77	100.24	98.58	99.93	99.50	99.27	99.63	99.82	99.87	99.26	99.12	99.34	99.63	99.32	99.12
Sc	2.1	3.0	2.5	2.4	5.1	4.1	3.7	3.2	3.9	33.5	27.5	24.4	24.7	28.9	29.8	22.4	9.8	24.3	41.7	16.6	9.8
Cr	197.7	210.4	311.3	428.2	319.8	302.9	214.4	307.2	336.1	112.2	75.7	92.4	13.5	114.4	238.2	376.2	280.5	180.6	174.1	210.0	274.3
V	246.3	254.4	262.5	333.6	238.7	186.8	184.9	193.0	241.1	255.4	271.7	279.3	248.6	293.7	314.0	266.4	295.0	240.3	218.7	285.2	315.7
Ni	137.0	144.0	151.0	157.9	121.4	159.1	148.9	171.5	178.4	44.8	38.7	31.8	14.8	40.6	55.1	98.2	73.2	92.7	93.5	71.6	86.1
Co	61.4	57.4	53.4	49.3	45.3	41.3	37.3	33.3	49.2	46.3	32.5	35.5	48.3	34.9	42.2	48.5	54.3	57.6	44.3	47.1	44.7
Cu	59.5	62.8	38.9	40.8	42.8	44.7	46.7	48.6	50.6	68.5	68.6	68.7	68.7	68.0	73.4	66.3	67.5	63.6	83.1	60.3	34.5
Zn	69.5	68.2	66.9	65.7	64.4	63.1	61.8	60.5	59.2	79.1	67.5	69.7	108.6	78.4	78.7	66.9	72.4	93.4	75.4	71.0	73.6
Ga	12.8	16.9	18.0	12.2	15.3	16.4	14.6	18.7	14.8	16.5	18.9	14.9	18.1	13.1	18.8	15.8	16.6	14.8	15.4	15.3	14.9
Rb	23.0	14.8	18.8	19.9	5.3	9.3	10.8	12.0	15.3	2.3	1.9	3.4	5.6	7.1	5.8	4.0	4.5	1.3	2.1	6.5	2.1
Sr	261.5	111.0	234.5	295.8	195.5	208.5	314.7	305.0	251.1	27.4	22.0	32.2	139.6	29.0	44.9	48.5	85.9	44.5	24.7	37.0	85.9
Y	33.55	34.55	43.46	35.44	27.62	19.51	19.90	21.26	30.78	22.85	20.30	24.51	22.85	23.76	22.01	21.62	22.26	20.70	15.12	23.94	22.23
Zr	254.19	254.76	346.62	320.13	145.98	118.65	134.17	169.85	213.66	43.28	43.36	49.52	50.08	61.55	46.99	44.46	42.59	39.71	30.12	47.06	53.99
Nb	66.59	61.04	97.80	89.88	31.67	19.18	26.75	39.84	47.51	2.69	2.62	2.86	3.50	3.38	2.96	2.08	2.33	2.01	1.31	2.53	2.07
Cs	0.96	0.20	0.30	0.50	0.30	0.40	0.33	0.40	0.50	0.08	0.04	0.21	0.19	0.11	0.15	0.12	0.20	0.04	0.06	0.13	0.20
Ba	494.20	350.60	271.34	435.42	67.00	119.00	157.00	224.77	308.50	20.20	17.80	47.80	37.20	35.80	51.18	41.94	42.50	16.30	19.00	74.50	32.50
La	45.80	47.80	68.50	59.38	19.24	10.67	14.52	23.86	34.02	4.38	4.09	4.62	5.28	5.26	4.06	3.78	3.25	2.95	1.87	4.42	3.29
Ce	91.33	103.09	136.59	124.63	39.10	24.70	29.13	51.45	73.44	10.61	11.47	11.27	12.19	12.48	13.50	10.52	8.16	8.83	5.22	5.65	8.78
Pr	11.44	11.94	17.12	13.38	5.05	3.08	3.67	6.00	8.55	1.55	1.45	1.68	1.90	1.90	1.50	1.46	1.31	1.18	0.86	1.59	1.38
Nd	46.97	46.02	65.25	52.15	21.25	13.19	15.15	24.88	35.44	7.62	7.31	8.55	9.32	9.46	7.65	7.38	6.65	6.13	4.51	8.02	7.00
Sm	9.02	8.83	12.09	10.88	4.97	3.15	3.28	5.28	6.89	2.37	2.07	2.66	2.70	2.76	2.34	2.32	2.17	1.98	1.46	2.43	2.21
Eu	2.65	2.79	3.67	3.31	1.51	1.06	1.00	1.67	2.15	0.85	0.73	0.96	0.93	0.97	0.85	0.85	0.78	0.71	0.55	0.88	0.81
Gd	7.05	8.07	9.62	8.99	4.31	3.32	2.89	4.91	5.60	3.10	2.67	3.45	3.35	3.51	3.12	3.11	2.89	2.62	2.01	3.23	2.98
Tb	1.03	1.08	1.59	1.15	0.71	0.47	0.51	0.70	0.84	0.56	0.48	0.64	0.60	0.62	0.58	0.56	0.53	0.48	0.38	0.58	0.53
Dy	5.40	5.64	8.08	5.51	3.97	2.73	2.68	3.57	4.50	3.53	3.10	4.28	3.94	3.87	3.63	3.75	3.36	3.11	2.59	3.99	3.41
Ho	1.02	1.16	1.53	1.11	0.78	0.63	0.54	0.75	0.94	0.86	0.72	0.92	0.87	0.90	0.85	0.83	0.78	0.75	0.58	0.89	0.81
Er	2.93	3.06	3.87	2.76	2.32	1.80	1.66	2.08	2.53	2.51	2.06	2.63	2.43	2.53	2.46	2.41	2.25	2.12	1.67	2.46	2.27
Tm	0.42	0.44	0.56	0.36	0.34	0.27	0.25	0.31	0.37	0.38	0.31	0.39	0.36	0.37	0.37	0.35	0.34	0.32	0.25	0.37	0.35
Yb	2.58	2.70	3.41	2.34	2.06	1.63	1.50	1.86	2.26	2.45	1.99	2.47	2.27	2.24	2.33	2.27	2.19	2.07	1.62	2.38	2.20
Lu	0.38	0.40	0.50	0.33	0.29	0.24	0.23	0.28	0.33	0.38	0.32	0.39	0.36	0.36	0.38	0.35	0.34	0.33	0.25	0.37	0.34
Hf	5.72	6.52	8.65	6.76	3.33	2.34	2.56	3.61	4.94	1.41	1.24	1.50	1.39	1.45	1.35	1.32	1.34	1.23	0.98	1.39	1.38
Ta	3.92	3.81	6.24	4.47	1.63	0.97	1.80	2.46	2.93	0.11	0.15	0.25	0.22	0.22	0.19	0.14	0.14	0.09	0.05	0.15	0.12
Pb	1.48	0.97	2.01	1.88	1.75	1.62	1.49	1.36	1.22	0.77	1.43	1.55	0.99	0.88	1.33	0.55	1.10	0.77	1.32	0.66	0.80
Th	4.40	3.73	7.01	6.72	1.58	1.10	1.77	2.83	3.86	0.37	0.41	0.63	0.74	0.72	0.72	0.71	0.84	0.35	0.13	0.72	0.54
U	1.61	1.73	3.20	3.21	0.60	0.63	1.13	1.41	1.56	0.14	0.15	0.23	0.27	0.21	0.23	0.21	0.22	0.13	0.05	0.22	0.18

Table 1. (continued)

Sample no.	TU14	AK11	AK12	AK13	AK15	AK40	AK41	AK24	AK21	AK28	AK32	AK34	AK3	AK9
Locality	Akhisar	Akhisar	Akhisar	Akhisar	Akhisar	Akhisar	Akhisar	Akhisar	Akhisar	Akhisar	Akhisar	Akhisar	Akhisar	Akhisar
Rock type	SSZ	SSZ	SSZ	SSZ	SSZ	SSZ	SSZ	SSZ	SSZ	SSZ	SSZ	SSZ	SSZ	SSZ
SiO_2	47.08	49.46	48.34	50.14	51.66	49.65	48.74	49.75	48.74	50.75	51.16	52.64	48.85	49.25
TiO_2	0.85	0.97	0.90	0.95	0.99	0.95	0.65	0.69	0.64	1.11	0.69	0.95	0.95	0.69
Al_2O_3	14.03	14.97	15.17	14.94	14.95	14.78	17.71	15.97	16.72	14.88	15.64	15.30	15.81	16.32
Fe_2O_3	11.33	10.96	11.98	10.52	11.49	11.41	9.83	9.89	9.83	11.18	10.38	10.49	10.92	9.90
MnO	0.17	0.18	0.17	0.18	0.21	0.19	0.16	0.17	0.17	0.19	0.16	0.18	0.16	0.16
MgO	8.21	6.44	6.94	7.39	6.27	6.63	7.96	7.87	8.10	6.36	6.12	7.26	6.79	8.15
CaO	9.95	9.03	9.38	9.25	6.48	8.43	8.37	9.17	9.18	8.33	8.30	6.12	9.19	9.10
Na_2O	3.45	3.42	2.89	2.96	4.14	2.79	2.59	2.17	2.15	2.73	3.17	2.90	2.79	2.18
K_2O	0.08	0.15	0.04	0.13	0.05	0.13	0.05	0.05	0.03	0.22	0.05	0.08	0.08	0.03
P_2O_5	0.12	0.09	0.09	0.09	0.09	0.11	0.05	0.06	0.06	0.15	0.06	0.09	0.09	0.06
LOI	4.20	3.70	3.80	3.10	3.50	4.28	3.72	3.25	3.87	3.85	3.40	3.75	4.20	3.21
Total	99.47	99.37	99.70	99.64	99.83	99.35	99.84	99.04	99.48	99.74	99.13	99.76	99.83	99.05
Sc	46.3	41.3	39.7	38.1	42.5	43.5	35.5	42.6	46.1	45.2	43.3	43.6	38.8	41.6
Cr	310.6	342.8	374.9	407.1	439.2	118.7	308.0	406.0	366.1	176.2	326.9	344.2	361.6	385.3
V	306.8	323.7	328.5	301.4	305.3	247.5	182.2	250.2	217.9	320.5	224.1	335.6	277.2	242.7
Ni	81.7	80.0	78.4	76.7	75.0	62.0	187.0	125.2	131.2	67.1	124.4	129.6	134.9	132.5
Co	46.0	45.5	44.9	44.4	43.8	52.7	53.4	43.1	43.2	40.5	36.2	32.7	29.3	42.7
Cu	62.1	59.0	64.0	58.3	55.7	36.9	34.3	44.5	41.9	45.8	48.3	29.9	31.4	32.9
Zn	78.3	79.1	80.0	80.8	81.7	81.1	58.6	61.2	57.5	74.6	58.8	55.8	52.9	61.4
Ga	14.6	14.4	14.2	13.9	13.7	16.6	15.5	14.0	13.6	15.5	13.8	13.4	13.0	13.9
Rb	1.9	5.5	0.9	3.3	1.1	3.2	1.1	0.7	0.6	5.3	2.7	23.8	14.5	1.7
Sr	340.9	202.6	10.0	180.7	104.2	123.8	108.0	95.7	84.5	138.7	154.0	117.4	128.5	95.8
Y	26.30	26.12	25.60	24.36	24.30	24.73	17.03	17.60	16.45	28.30	17.23	23.62	24.70	17.89
Zr	45.87	52.11	49.30	43.10	44.16	46.44	27.49	35.64	30.75	65.35	30.08	54.59	42.81	33.38
Nb	1.96	2.15	1.94	1.99	2.08	2.69	0.74	0.92	0.79	4.15	0.90	1.86	1.54	0.86
Cs	0.20	0.20	0.10	0.30	0.10	0.05	0.05	0.10	0.01	0.09	0.06	0.50	0.70	0.11
Ba	19.02	76.04	10.02	34.07	12.02	32.63	17.06	17.90	6.66	66.82	16.08	97.13	75.04	16.25
La	3.26	3.65	3.37	3.16	3.26	3.43	1.16	1.41	1.33	7.44	1.44	3.04	2.83	1.51
Ce	8.45	9.14	8.47	9.16	8.42	9.11	3.56	3.85	4.06	14.38	4.34	4.69	7.65	8.28
Pr	1.36	1.51	1.35	1.36	1.33	1.39	0.63	0.78	0.71	2.12	0.76	1.32	1.29	0.75
Nd	7.47	8.59	7.75	7.67	7.58	7.79	4.03	4.92	4.54	10.81	4.64	7.59	7.50	4.73
Sm	2.49	2.57	2.39	2.29	2.28	2.26	1.34	1.53	1.46	3.03	1.47	2.32	2.35	1.57
Eu	0.91	0.95	0.88	0.87	0.86	0.84	0.52	0.59	0.56	1.08	0.56	0.85	0.87	0.61
Gd	3.39	3.49	3.26	3.11	3.11	3.09	1.99	2.22	2.04	3.79	2.06	3.04	3.17	2.24
Tb	0.62	0.64	0.61	0.58	0.58	0.57	0.36	0.42	0.37	0.68	0.39	0.57	0.58	0.43
Dy	4.30	4.36	3.93	3.72	4.02	4.01	2.51	2.70	2.74	4.64	2.52	3.67	4.07	3.01
Ho	0.96	0.96	0.92	0.88	0.90	0.88	0.59	0.64	0.61	0.98	0.59	0.87	0.90	0.66
Er	2.81	2.81	2.59	2.56	2.55	2.48	1.81	1.85	1.78	2.61	1.71	2.38	2.52	1.93
Tm	0.42	0.42	0.40	0.39	0.39	0.38	0.25	0.27	0.26	0.38	0.26	0.37	0.39	0.29
Yb	2.31	2.36	2.17	2.16	2.20	2.08	1.44	1.48	1.50	2.09	1.49	1.95	2.16	1.59
Lu	0.42	0.43	0.39	0.37	0.39	0.36	0.26	0.26	0.27	0.38	0.26	0.35	0.37	0.28
Hf	1.35	1.54	1.46	1.41	1.39	1.37	0.84	0.97	0.96	1.52	0.91	1.32	1.40	0.95
Ta	0.11	0.14	0.13	0.14	0.12	0.18	0.04	0.07	0.07	0.17	0.08	0.08	0.11	0.04
Pb	0.69	0.63	0.56	0.50	0.44	0.77	1.43	1.02	1.01	1.37	0.62	1.15	0.67	0.04
Th	0.18	0.22	0.21	0.27	0.28	0.31	0.09	0.13	0.11	0.57	0.13	0.19	0.13	0.14
U	0.06	0.09	0.05	0.12	0.04	0.10	0.04	0.03	0.02	0.24	0.04	0.06	0.06	0.03

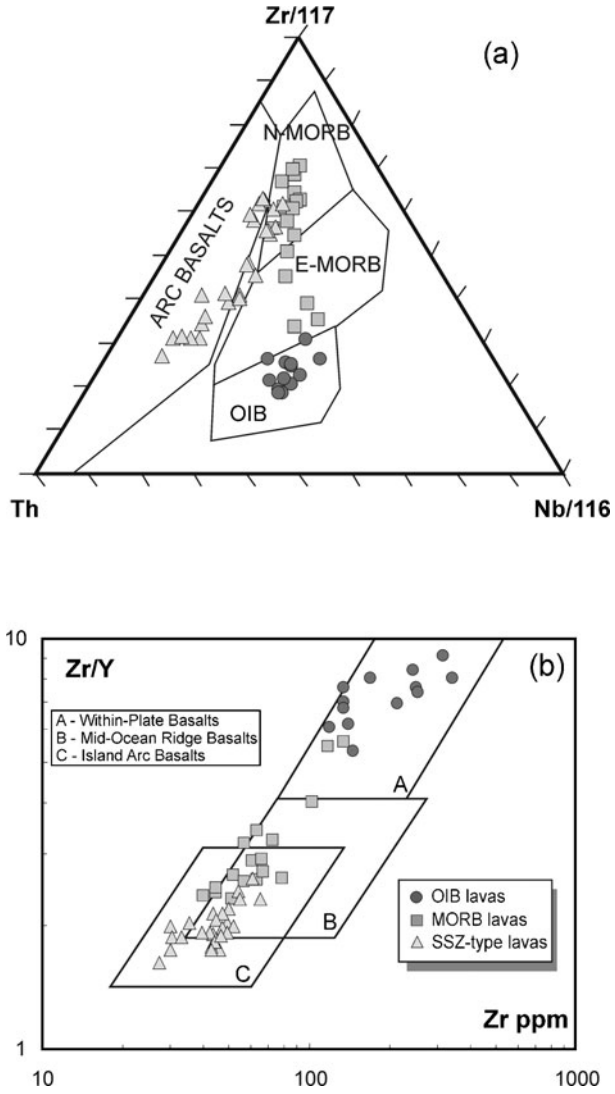

Figure 2. (a) Zr/117–Nb/16–Th diagram showing the basaltic lavas with respect to the fields for within-plate basalt (WPB), volcanic-arc basalt (VAB), normal (N) MORB and enriched (E) MORB (after Wood, 1980). (b). Zr/Y v. Zr discriminant diagram for the basaltic lavas within the Tethyan suture zone in western Turkey. The fields of within-plate basalt (WPB), mid-ocean ridge basalt (MORB) and island arc basalt (IAB) are from Pearce & Norry (1979).

subduction-related basalts and hence plotting in the field of volcanic arc basalts (Fig. 2a). The samples as a whole form two distinct trends defined by MORB–OIB and MORB–arc basalt compositions. The latter constitutes the SSZ-type lavas. In the Zr/Y v. Zr discrimination diagram, the samples also form a range of compositions in the fields of mid-ocean ridge basalt (MORB), within-plate basalt (WPB) and the island arc basalt (IAB) (Fig. 2b).

The MORB suite shows a significant fractionation range, and has Zr and Nb contents from 40 to 135 ppm and 1 to 18 ppm, respectively. The majority of the MORB basalts have Ti/Zr (90–120) and La/Nb (0.80–1.28) values characteristic of N-MORB, but enriched-type MORB (E-MORB) compositions with greater incompatible to less incompatible element ratios also exist. The classification of the basalt types shown in Figure 2a and b is detailed below, with reference to average normal MORB- and CI chondrite-normalized trace element plots.

4.c. Normalized multi-element and REE plots

In Figure 3 the samples are plotted on multi-element variation diagrams normalized to the average MORB

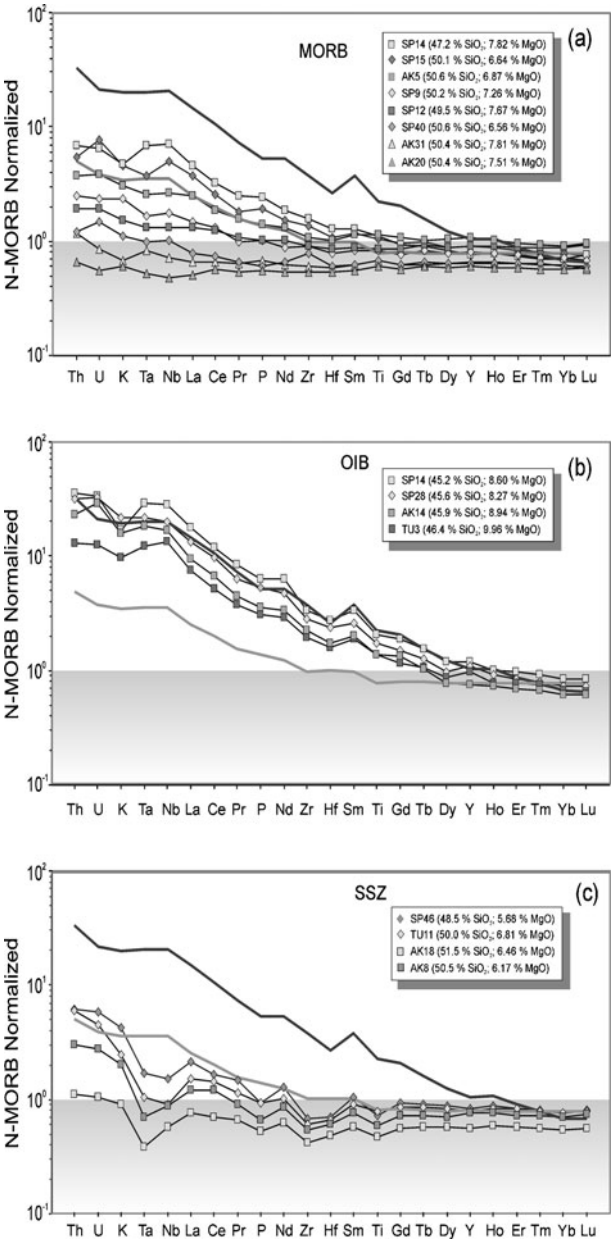

Figure 3. N-MORB normalized multi-element patterns for the (a) MORB-, (b) OIB- and (c) SSZ-type basaltic lavas from the Tethyan suture zone in western Turkey. Average E-MORB and OIB compositions are shown by grey and dark heavy lines, respectively. E-MORB, OIB compositions and N-MORB normalizing values are from Sun & McDonough (1989).

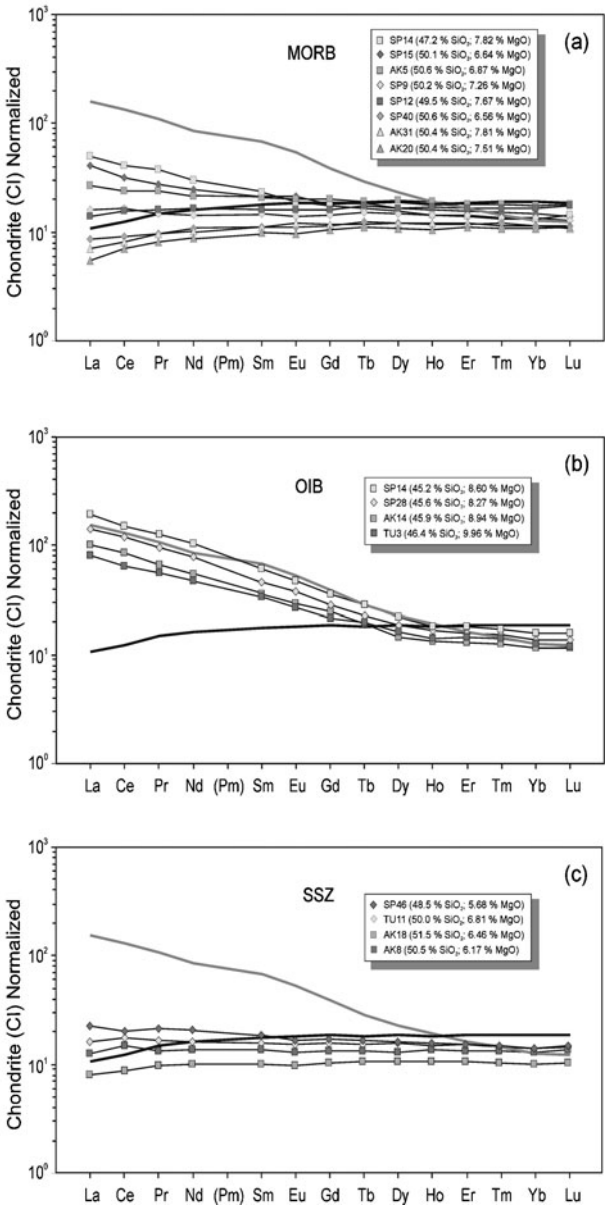

Figure 4. Chondrite-normalized REE element patterns for the (a) MORB-, (b) OIB- and (c) SSZ-type basaltic lavas from the Tethyan suture zone in western Turkey. Chondrite normalizing values are from Boynton (1984). Average N-MORB and OIB compositions are shown by dark and grey heavy lines respectively. N-MORB and OIB compositions are from Sun & McDonough (1989).

compositions of Sun & McDonough (1989). Also plotted for comparison are some typical oceanic basaltic compositions, including the enriched MORB and ocean island basalt (OIB) compositions of Sun & McDonough (1989). Corresponding chondrite-normalized REE plots are also presented in Figure 4.

The MORB lavas, with their variable enrichments and depletions in incompatible trace elements, exhibit a compositional range between N-MORB and E-MORB (Fig. 3a). The N-MORB varieties display patterns close to the sub-horizontal patterns followed by average N-MORB composition of Sun & McDonough (1989). On a plot of chondrite (CI)-normalized REE, these rocks are characterized by LREE-depleted and rather steeper middle to heavy REE patterns. The rocks have fractionated LREE to MREE patterns ($(La/Sm)_N = 0.55–0.97$, where the subscript N denotes normalization to CI chondrite), which characterize basaltic lavas from oceanic spreading centres or marginal basins where basalt compositions can be modelled in terms of partial melting of melt-depleted mantle source with a possible involvement of slight proportions of enriched components (e.g. Niu *et al.* 2002; Leat *et al.* 2004). The E-MORB varieties, on the other hand, display a progressive enrichment in incompatible elements relative to N-MORB compositions, with a degree of enrichment that increases systematically with increasing incompatibility, resulting in smooth negative slopes in chondrite-normalized REE plots (Fig. 4a). The ratios of $(La/Sm)_N$ for the E-MORB-type rocks range between 1.08 and 2.14 and are comparable to those observed in basalts from spreading centres in the proximity of relatively enriched mantle domains, such as in Iceland (Slater *et al.* 2001) and some seamounts near the East Pacific Rise (Niu *et al*. 2002).

The alkaline basalts have Nb contents at least twice those of the MORB-like suite at a similar degree of fractionation, but have lower Zr/Nb values in a range between 3.54 and 6.19. Normal-MORB normalized element variation patterns for the alkaline rocks show significant enrichment in the more incompatible elements. The samples mostly fall between those of enriched ridge-generated MORB (e.g. E-MORB) and the average ocean island basalt (OIB), but the samples with greater enrichments in incompatible elements than the average OIB also exist. The rocks of this suite have all the classic enrichments in LILE, HFSE and L-MREE and slight depletion in HREE (e.g. relative to the average N-MORB) that characterize basalts from intra-plate oceanic settings (Fig. 3b). The rocks, however, display slight negative anomalies in Zr, Hf and Ti with respect to the neighbouring incompatible elements in Figure 3b. In chondrite-normalized plots the alkaline rocks have almost straight and sub-parallel REE patterns with near-constant concentration ratios (Fig. 4b). We interpret these basalts of intra-plate origin as having originated from a geochemically enriched (in terms of incompatible elements) component, possibly formed as seamounts on ocean crust.

The SSZ tholeiites show prominent depletions in high field strength elements relative to fluid-mobile elements (e.g. negative Ta and Nb anomalies with respect to the neighbouring incompatible elements) on a MORB-normalized plot (Fig. 3c). These characteristics are common in arc environments and mostly ascribed to subduction enrichment and fluid metasomatism processes in subduction zones (e.g. Pearce *et al.* 1995). The lavas, however, are slightly depleted in some HFSE and HREE and enriched in LREE with respect

to N-MORB, which may be interpreted as reflecting generation of melt from a source that is depleted by previous melt extraction and subsequently enriched in subduction-mobile incompatible trace elements. The rocks have relatively enriched REE patterns with $(La/Sm)_N$ between 0.95 and 1.24 and $(La/Yb)_N$ between 0.92 and 1.63. Primary and slightly evolved lavas exhibit sub-parallel REE parents, suggesting that the latter have experienced shallow-level crystal fractionation of their plagioclase, pyroxene and olivine phenocrysts. Overall, the trace element characteristics of the lavas exhibit strong similarities to those formed in oceanic basins near convergent plate boundaries, where the influence of a marked subduction component signifies the geochemical characteristics of the source mantle (e.g. Taylor & Martinez, 2003; Leat *et al.* 2004; Pearce *et al.* 2005).

5. Evaluation of mantle sources and melting processes

5.a. Th/Yb v. Ta/Yb and Ta/Nd v. Th/Nb plots: evidence for multiple enrichment of the mantle source

Ratios of incompatible elements with similar incompatibilities highlight mantle source variations and allow determination of the relative importance of melt extraction and mantle metasomatism in the geochemical characteristics of mantle-derived melts. An examination of incompatible trace element behaviour of the lavas has been performed to define the source variations of the lavas using the Th and Ta concentrations (Fig. 5). Ytterbium is used as a normalizing factor to minimize the effects of fractional crystallization and crystal accumulation (e.g. Pearce & Peate, 1995; Pearce *et al.* 2005).

A projection of Th/Yb versus Ta/Yb (Fig. 5) defines three different rock assemblages with reference to the classification made in Figure 2. Among these, the rocks with MORB geochemical signatures contain both N-MORB and E-MORB compositions. Thorium and Ta have similar distribution coefficients for melting and fractional crystallization, so that MORB forms a diagonal array on the projection in Figure 5 with a slope close to unity. Extremely large variations in both Th/Yb and Ta/Yb ratios for the MORB suite suggest that these subduction-unmodified lavas can be interpreted to have originated from mixing of melts from sub-lithospheric sources with variable, but systematic, enrichments in incompatible trace elements, and are likely to define the local MORB array of increasing Th/Yb with increasing Ta/Yb. Higher values in both Th/Yb and Ta/Yb ratios for some samples (E-MORB in particular) may be explained by the involvement of an incompatible element enriched component in their source mantle.

The OIB-type alkaline rocks are characterized by strong enrichments in highly incompatible elements

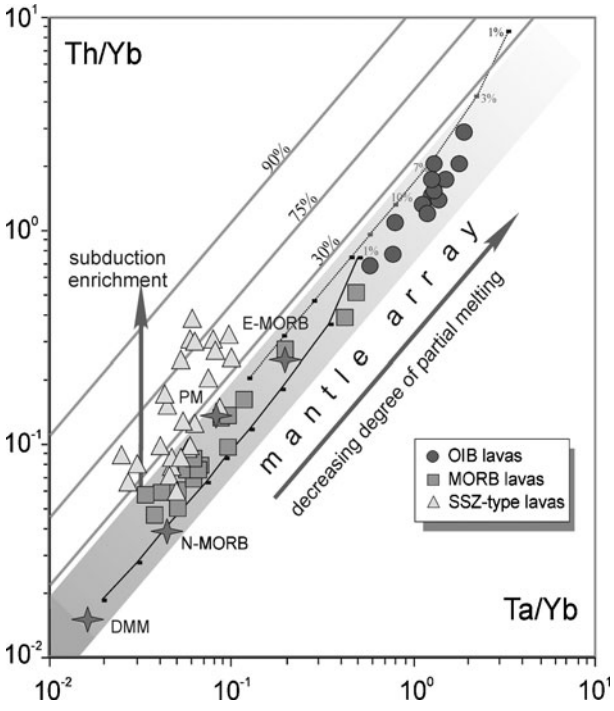

Figure 5. Plot of Th/Yb v. Ta/Yb for the MORB-, OIB- and SSZ-type basaltic lavas from the Tethyan suture zone in western Turkey. Also plotted for comparison are some typical oceanic basaltic and mantle compositions including the depleted MORB mantle, primitive mantle (PM), N-MORB and E-MORB. Partial melting trends predicted using the depleted MORB mantle and PM compositions as the source are shown as solid lines with the calculated degrees of melting on each curve (shown as thick marks). Contours parallel to the mantle array denote the percentage of subduction-derived element Th in the mantle source, assuming that Ta is subduction-immobile (e.g. Pearce *et al.* 2005).

relative to less incompatible elements (e.g. higher LREE/HREE ratios than that of MORB). They plot on the MORB–OIB mantle trend on a Th/Yb v. Ta/Yb diagram, indicating that their mantle source had no subduction influence and the resulting magmas were not affected by any significant contamination of lithospheric material. Higher ratios of both Ta/Yb and Th/Yb relative to MORB compositions, however, may be explained by a number of processes including magma generation by: (1) small degrees of melting of a convectively homogenized source that is enriched in incompatible elements relative to depleted MORB source; or (2) small degrees of partial melting of a mantle source that leaves garnet-bearing residue (e.g. Aldanmaz *et al.* 2000); or (3) systematic mixing between increments of melt derived from a compositionally uniform source by variable degrees of melting (e.g. Aldanmaz, Gourgaud & Kaymakci, 2005; Aldanmaz *et al.* 2006).

The SSZ tholeiite lavas exhibit clear displacements from the MORB–OIB array to higher subduction-mobile element Th. It is known that Ta/Yb ratios are not affected, or little affected, by additions of components

during plate subduction, whereas an increase in Th/Yb, due to the introduction of additional Th into the source, reflects additions of slab-derived components (Pearce *et al.* 1995). These components are widely thought to be crust-derived aqueous fluids and sediment-derived siliceous fluid, that is, supercritical fluid or melt (Pearce *et al.* 1995; Hawkesworth *et al.* 1997). The addition of a subduction component to a constant mantle source would be expected to give a vertical trend on the diagram, as only Th is added while Ta and Yb remain nearly constant. However, the SSZ tholeiites from the ophiolitic suites of western Turkey form a trend that diverges sub-vertically from the MORB array, indicating that variable contribution from a subduction-enriched component has strongly influenced the mantle source chemistry.

The compositional effects of the slab-derived components and enriched versus depleted mantle sources on the oceanic basalts can also be investigated using the plot of Ta/Nd versus Th/Nb (Fig. 6). Two distinct trends in the diagram diverge strongly from N-MORB compositions. One of these trends is defined by MORB–OIB compositions and characterized by increasing Ta/Nd ratios at near constant Th/Nb. This trend could be the result of mixing between melts from MORB- and OIB-type sources, or alternatively, variable degrees of partial melting of a source similar in composition to the depleted MORB mantle. The second trend, on the other hand, displays increases in Th/Nb ratios with no significant change in Ta/Nd. This horizontal trend, which is defined by the compositions of SSZ tholeiite lavas, can be interpreted to represent MORB-subduction component mixing, or addition of subduction component to the depleted MORB mantle source prior to mantle melting to produce oceanic crust with composition resembling typical back-arc basin lavas.

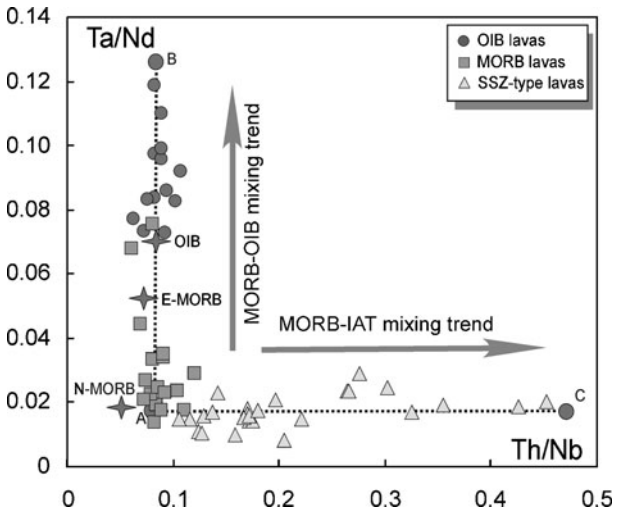

Figure 6. Variation of Ta/Nd with Th/Nb for the MORB-, OIB- and SSZ-type basaltic lavas from the Tethyan suture zone in western Turkey. The predicted mixing trend between MORB and OIB compositions defines the vertical trend comprising the compositional variations of the MORB- and OIB-type lavas from western Turkey, while the model prediction constituting the subduction influx into the depleted MORB mantle can account for the compositions of the lavas with SSZ geochemical signatures. End-member components shown in the figure are defined by 17 % melting of a depleted mantle source (A), 4 % melting of an enriched mantle source (B) and 20 % melting of a subduction-enriched mantle source (C).

5.b. La/Yb v. Zr/Nb and La/Sm v. La plots: modelling source characteristics of the MORB- and OIB-type lavas

In Figures 7 and 8 we attempted to model numerically the REE and Zr and Nb abundances and ratios in an effort to constrain the source variations in the genesis of subduction-unmodified (e.g. MORB- and OIB-type) lavas from the ophiolitic suites of western Turkey. Ratios of highly incompatible trace elements such as La/Sm or Zr/Nb in tholeiitic and alkali basalts provide constraints on their source chemistry and degree of melting because these ratios are unlikely to be strongly fractionated by mineral separation (Aldanmaz, 2002). Therefore, the variation in such ratios in basalts from oceanic basins can be used to document the range of source compositional variations present beneath oceanic spreading systems or seamounts.

Using the approach by Aldanmaz (2002) and Aldanmaz *et al.* (2006), it is shown by plots of La/Sm v. La and La/Yb v. Zr/Nb that MORB and OIB types of basalts are unlikely to have originated from the same source, if melt production is considered in the conventional context of single-stage melting and instantaneous melt extraction (Figs 7, 8). The modelling shows that although some of the N-MORB compositions from the ophiolitic suites of western Turkey can be generated by 10–15 % melting of a source similar to depleted MORB mantle, the majority of the rocks display compositional trends that are different from the model liquid compositions (or melt extraction trajectories) produced using depleted MORB mantle as the source composition. In particular, most of the E-MORB and the OIB compositions have highly incompatible to less incompatible element ratios (e.g. La/Sm and Nb/Zr) greater than those that could be generated by a single-stage melting of depleted MORB mantle, even when the degree of partial melting is taken to be unrealistically small (e.g. 0.01 %).

Figure 8 further illustrates that the MORB lavas define a linear trend on a La/Sm v. La diagram with a depleted end-member representing N-MORB composition formed by about 15 % melting of depleted MORB mantle and an enriched end-member representing the most enriched E-MORB formed by melting of a mantle component enriched in incompatible elements. The lavas representing the entire spectrum of the MORB suite can therefore be interpreted as resulting from mixing between an enriched (defined by some of the enriched E-MORB and the entire spectrum of

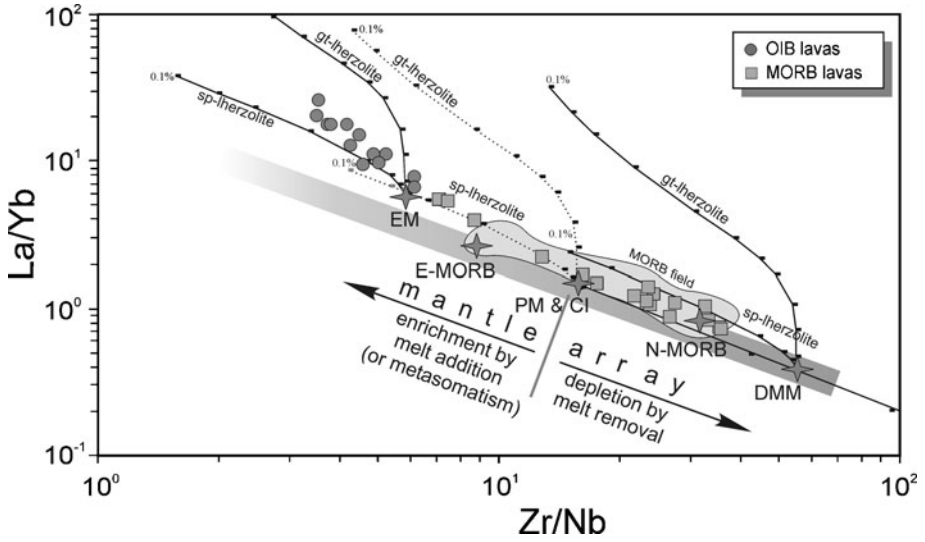

Figure 7. Plot of La/Yb v. Zr/Nb showing melt curves (or lines) obtained using the non-modal batch melting model (see Aldanmaz *et al.* 2000 and Aldanmaz, 2002 for details). The parameters and common geochemical reservoirs used in the diagram are as described in Aldanmaz *et al.* (2000). The enriched mantle (EM) is assumed to have incompatible element concentrations similar to that proposed in Aldanmaz *et al.* (2006). The mantle array is defined using melt-residual compositional trends from depleted MORB mantle (DMM) and primitive mantle (PM; similar in composition to CI chondrite) compositions. Mantle depletion and enrichment trends are defined by melt extraction from the mantle (towards the residues) and melt addition to the mantle (or influx of material from outside the mantle prior to solid-state mixing and homogenization) respectively. The melting trends from depleted MORB mantle and enriched mantle compositions are shown by solid curves (or lines) while the dashed curves (or lines) represent the melting trends from primitive mantle. Thick marks on each curve (or line) correspond to degrees of partial melting for a given mantle source. MORB field defines the compositional range of basalts from the East Pacific Rise (Niu *et al.* 2001).

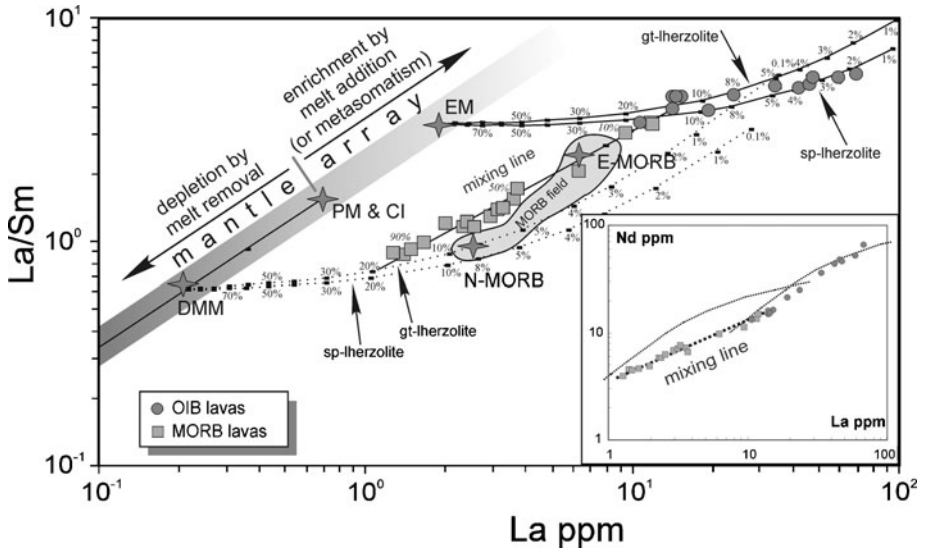

Figure 8. Plot La v. La/Sm showing melt curves (or lines) obtained using the parameters described in the caption of Figure 7. The straight line array represents a mixing line between melts from enriched (e.g. enriched mantle, EM) and depleted (e.g. depleted MORB mantle) components. The numbers in italic denote the mixing proportion of the depleted component in the final melt produced. The inset diagram compares the variations of highly versus moderately incompatible elements (La v. Nd) for the MORB- and OIB-type lavas from the ophiolitic suites of western Turkey with model partial melting curves (or lines) for both depleted and enriched mantle components obtained assuming the non-modal batch melting model. Continuous partial melting of any single source predicts curved trends for moderately versus highly incompatible elements. In contrast, highly and moderately incompatible trace elements from the MORB and OIB lavas from western Turkey generally exhibit individual quasi-linear trends suggesting a mixing between melts derived from sources with different compositions. Descriptions of geochemical reservoirs are as given in Figure 7.

OIB-type lavas) and a depleted (defined by the N-MORB lavas) component. Because the concentrations of incompatible trace elements in the two sources are remarkably different, only 1–2 % of enriched component is needed to overwhelm the trace element characteristics of the lavas resembling typical N-MORB, while the compositions of the most enriched E-MORB- and OIB-type lavas can be explained by

melting of the enriched component with slight or no contribution from the depleted component.

Model predictions show that the majority of the N-MORB and E-MORB compositions can be produced by systematic mixing of melts produced by variable degrees of partial melting of these two compositionally distinct sources. In this context, 'melting-induced mixing' of at least two-component mantle can be considered a viable mechanism to produce the compositional spectrum observed in these subduction-unmodified ophiolitic lavas. The process envisioned resembles that proposed to explain mantle melting and melt extraction in many extensional settings including oceanic spreading systems, back-arc environments and continental break-up settings (Cousens *et al.* 1995; Niu *et al.* 2002; Meibom & Anderson, 2003; Pearce, 2005; Korenaga, 2004).

6. Petrogenetic considerations

6.a. Heterogeneous MORB–OIB source and multi-component mantle melting

It is a common notion that MORB lavas are remarkable for their tremendous chemical homogeneity (e.g. Dupre *et al.* 1981; Hofmann, 1997). Almost all MORB are olivine-normative tholeiites with a significantly restricted range in major and trace element compositions, motivating many workers to treat the MORB source as a large-scale homogeneous reservoir. However, numerous studies from presently active oceanic spreading systems have demonstrated that the chemical variability of ocean floor basalts dramatically increases for samples not erupted at established ridge axes, and significant chemical variations in oceanic basalts occur in relatively short time- and length-scales (e.g. Cousens *et al.* 1995; Niu, Collerson & Batiza, 1999; Lundstrom *et al.* 1999; Donnelly *et al.* 2004; Graham *et al.* 2006).

The observed trace element compositional diversity between the sources of N-MORB- and E-MORB- (and OIB)-type magmas is, in general, evident by relative enrichment of E-MORB- and OIB-type sources in more incompatible over less incompatible elements. This clear chemical distinction is essentially the common characteristic of the vast majority of OIB and E-MORB suites and could best be explained by the upper mantle compositional heterogeneities and the existence of enriched components. This would allow the chemical composition of enriched magmas to be explained in terms of involvement of two or more chemically distinct end-members, which requires that the mantle comprises a mixture of enriched and depleted components (e.g. Schilling, 1973; Allègre & Turcotte, 1986; Sleep, 1984; Cousens *et al.* 1995; Meibom & Anderson, 2004; Ito, Lin & Graham, 2003; Pearce, 2005; Debaille *et al.* 2006).

The trace element modelling presented above shows that the melt compositions forming the temporally associated, subduction-unmodified basaltic lavas from the ophiolitic suites of western Turkey display geochemical trends that change from N-MORB through E-MORB to OIB-type magmas. In particular, the MORB suite exhibits a compositional trend that ranges from LREE-depleted to extremely LREE-enriched varieties. The variations in incompatible element concentrations and ratios among different types of MORB (and OIB) compositions are too large to be explained by either fractional crystallization from a single parental melt or melting of a single, chemically uniform mantle source. Moreover, E-MORB lavas are broadly similar in major element composition to N-MORB, with some subtle differences. This may indicate that E-MORB and N-MORB may result from similar degrees of melting, meaning that higher incompatible element concentrations and different trace element ratios in E-MORB are likely inherited from their source.

The model liquid compositions produced using concentrations and ratios of highly incompatible and less incompatible trace elements (e.g. La/Sm v. La, and La v. Nd) are expected to form curvilinear trends (Fig. 8). This is consistent with the theoretical assessment of mantle melting, which requires the rate of depletion of the highly incompatible element with progressive melting to be significantly higher than that of the less incompatible element. The MORB- and OIB-type ophiolitic lavas from western Turkey, however, are represented by two distinct straight line arrays rather than curvilinear trends, suggesting that magma generation by continuous melting from a single mantle source is difficult to reconcile with the incompatible trace element relationships of these lavas.

The simplest explanation for the correlations shown in Figure 8 is mixing of melts from a heterogeneous source region. Such correlations between highly incompatible trace element abundances (or ratios) indicate that N-MORB, E-MORB and OIB compositions are intimately linked in the melting process and that at least two distinct mantle sources, one similar to the depleted MORB mantle and the other more enriched than the depleted MORB mantle, must participate in generating the basalts with MORB and OIB compositions.

The concentration relations within the MORB and OIB suites suggest that typical E-MORB reflects a mix of 75 % OIB and 25 % N-MORB. The overall higher ratios of the highly to less incompatible elements of the samples probably reflect a greater contribution from the OIB-like end-member, or sometimes even OIB formation, which can be explained by diminished amounts of melt derivation from the depleted source, probably due to the integrated effects of conductive cooling and insufficient pressure release away from the ridge axis. The relatively homogeneous chemical composition of N-MORB, however, may simply reflect mixing that occurs because of magma focusing and

passage through axial melting regions in spreading centres, which result from efficient homogenization of melts at the ridge axis where melt generation is dominated by a relatively large extent of melting (about 15 %) of a depleted component. It is therefore reasonable to expect N-MORB (depleted) formation at the ridge axis and E-MORB or even OIB-type compositions (enriched) away from the axis (e.g. off-axis sea mounts).

6.b. Origin of subduction component in producing SSZ-type tholeiites in an oceanic basin

A distinctive geochemical feature of many back-arc magmas is the depletion in HFSE, enrichment in LILE, and common enrichment in LREE relative to N-MORB compositions. Since both HFSE and LILE behave incompatibly during partial melting of mantle rocks, this characteristic is difficult to reconcile with a single-stage melting and melt extraction from a source with geochemical characteristics similar to that of the ambient MORB mantle. Thus, it is commonly suggested that more than a one-stage melting process is required to explain geochemical characteristics of back-arc basin basalts (e.g. McCulloch & Gamble, 1991; Woodhead, Eggins & Gamble, 1993; Pearce *et al.* 2005). The commonly used model predictions suggest that the initial stage of melt extraction depletes the source in all incompatible trace elements (e.g. LILE and HFSE), leaving a depleted and refractory mantle residue. A subsequent melting occurs after, or during, a hydrous LILE (and LREE)-enriched but HFSE-depleted component, most probably a subduction component, is added to the source mantle.

The existence of SSZ-type tholeiites with geochemical signatures indicative of pre-melting subduction influence provides evidence for the development of arc-like crust by the inferred second-stage melt generation. In particular, geochemical data from some of the basaltic rocks from the ophiolitic units of western Turkey require generation from a relatively refractory source (depleted in HFSE and REE), most likely residual from previous melting and MORB extraction that was subsequently enriched in subduction-mobile LILE and LREE.

The origin of oceanic crust with arc-like geochemical signatures can therefore be explained by a mechanism in which an influx of aqueous fluids (or siliceous melts) carrying the subduction-related enriched components (e.g. rich in mobile incompatible elements) triggers a second-stage melting event in the SSZ residual mantle that had previously yielded MORB-type melts at the spreading centre. This depleted and subsequently enriched mantle domain may undergo either simple decompression or flux-induced melting at the spreading centre to produce basaltic magmas with convergent margin geochemical signatures.

The relative importance of siliceous melts and aqueous fluids in creating subduction components in SSZ mantle melting regions can be examined using Hf–Nd systematics. In particular Hf–Nd variations can be used to understand the HFSE anomalies that characterize magmas produced along convergent plate boundaries and modelling of mixing trends on Hf–Nd element plots places constraints on the Nd/Hf ratio in the subduction component. With their similar incompatibilities HFSE and REE are generally expected to behave coherently in mantle melting systems where relatively homogenized mantle domains melt to produce MORB and OIB magmas. In areas of plate convergence and subduction, however, relative enrichment in REE results in negative anomalies in Hf concentrations with respect to Nd (e.g. Thirlwall *et al.* 1994; Pearce & Peate, 1995).

Pearce *et al.* (1999) suggest that a Hf/Yb–Nd/Yb plot can be used to provide constraints on possible roles of slab-derived components (e.g. aqueous fluids released from the slab during dehydration or silicate melts generated by partial melting of slab components) in creating convergent margin geochemical signatures. On a log–log binary plot, these element ratios give a straight-line relationship and form a horizontal mantle trend if the basaltic melt is produced by partial melting of ambient mantle compositions (e.g. MORB–OIB production). Displacements from the mantle trend, however, should be associated with addition of components having Nd/Hf ratios different from the ambient mantle-derived melt compositions.

Most of the SSZ-type lavas from the ophiolitic suites of western Turkey are displaced from the 'mantle array' defined by MORB–OIB compositions toward the lower Hf/Yb (Fig. 9), consistent with their slight to moderate negative Hf anomalies (δHf < 1). Hafnium anomalies shown by these samples seem to be consistent with the addition of a subduction-related component, in which the Nd/Hf ratio exceeds a value of about 20, or approximately five times that of the local MORB source (Fig. 9). It is suggested that Hf, although soluble to varying degrees in siliceous melts, has a low solubility in aqueous fluids derived from subducted materials and is unlikely to have been transported to the mantle in fluids originated from slab dehydration (e.g. Barry *et al.* 2006). In contrast, Nd is more soluble in both subduction-derived fluids and melts. Thus, elevated Nd/Hf ratios in slab-derived fluxes would be inconsistent with melting of sediment or oceanic crust, but could only be explained if aqueous fluids dominated subduction-related inputs to the basalt source region (e.g. Pearce *et al.* 1999). The data suggest that the SSZ-type tholeiitic lavas sampled from the ophiolitic suites of western Turkey are the products of melting of depleted MORB mantle which presumably interacted with subduction fluid originated largely from processes of slab dehydration.

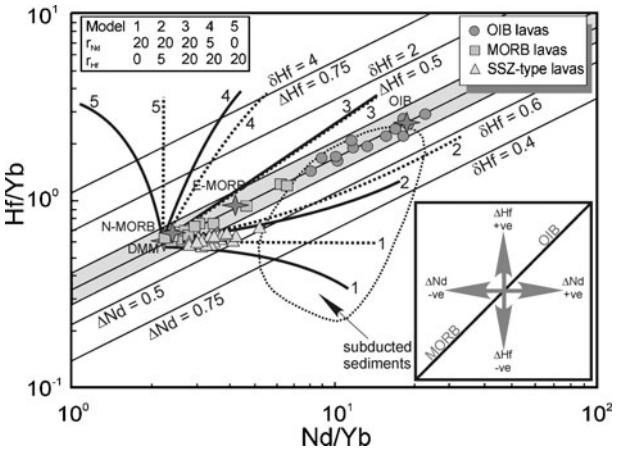

Figure 9. Hf–Nd co-variations (after Pearce *et al.* 1999) in the basaltic lavas from the Tethyan suture zone ophiolites in western Turkey. ΔHf and ΔNd define extent of positive and negative displacements of samples from the mantle array (shown as shaded area) defined by average MORB–OIB compositions (Pearce *et al.* 1999). Δ values indicate displacements from the mantle array and positive Δ value corresponds to high element ratios with respect to the mantle array. Equal Hf anomalies (δHf) are represented by straight lines parallel to the MORB–OIB array, with positive ΔNd values corresponding to negative Hf anomalies. Positive ΔNd values record the proportion of subducted Nd in mantle sources. δHf describes the negative Hf anomaly as a Hf depletion (that is, $\delta Hf < 1$), whereas ΔNd describes the anomaly as a Nd enrichment. Both ΔHf and ΔNd can be expressed in terms of the element compositions of the mantle and subduction zone end-members. Mixing trends between depleted MORB mantle (DMM) and subducted pelagic sediment (see Pearce *et al.* 1999 for detail) are also shown for a mass fraction of subduction component in the mantle between 0.05 and 0.2 and a range of values of r_{Nd} and r_{Hf} at r_{Yb} equal to 0 (dashed lines) or 2 (solid lines). Representative ratios (r) for Hf and Nd between the subduction component and the mantle are shown as inset.

7. Remarks on the tectonic setting of crust generation

Because the lavas from the ophiolitic suites of western Turkey are largely accreted fragments of oceanic crust, their sampling locations may not be representative of the entire spread and nature of this particular oceanic basin. Therefore, it is difficult to evaluate the temporal geochemical changes of magmatic events that took place over the entire history of the oceanic basin. However, it is possible to identify individual mantle source components that contributed to the processes of crust generation and the relevant tectonic setting in which the oceanic crust formation took place.

Spatial or temporal modification of the magmatic affinities in ophiolites is usually thought to reflect the variation of the geotectonic setting of the primary magma source. Existence of basaltic extrusive rocks with clear geochemical distinctions within the ophiolitic suites of this study may therefore indicate more than one stage of crust generation in an oceanic environment. One of these stages is marked by the formation of lavas with MORB–OIB geochemical signatures and can be modelled by interaction between melts from at least two end-member components, each with its own chemical homogeneity. The magmatic processes during this stage are rather similar to those observed in presently active oceanic spreading systems (e.g. the East Pacific Rise: Niu *et al.* 2002) where melt production is characterized by multi-component mantle interaction and mixing of melts from variably enriched and depleted mantle domains. This stage therefore can be described as the opening stage of an oceanic basin where the crust production is dominated by along-axis pressure-release melting of depleted MORB mantle with some contribution from off-axis melting of more enriched sub-lithospheric sources.

The other stage, however, is remarkable for the formation of SSZ-type basalts and involves melt contribution from a subduction-modified upper mantle source. This stage requires oceanic crust generation in association with plate convergence, most probably along a SSZ-type spreading centre, that is, the upper plate at a convergent plate boundary (Miyashiro, 1973; Pearce, 2003). The tholeiitic lavas produced during this stage are usually characterized by their relative depletion in subduction-immobile HFSE elements and enrichment in Th compared to average N-MORB. In some places, the subduction-enriched and MORB-type lavas are in close association, but there is no evidence that the subduction-enriched tholeiites were built onto an older MORB crust, indicating that the SSZ-type magmas were probably generated at the same oceanic spreading centre from which the adjacent MORB-type crust formed. The lack of volcanic arc associations directly overlying the MORB basalts within these ophiolitic suites and scarcity of magma compositions toward more evolved silicic intermediate rock types (e.g. andesites) may further indicate that the SSZ-type tholeiitic basalts formed in a supra-subduction-type oceanic spreading centre, rather than in a volcanic arc environment.

Possible scenarios for the addition of a subduction component into the mantle melting region and for melt generation beneath an oceanic spreading system include: (1) influx of the subduction fluid directly into the melting zone beneath the MORB-like lithosphere, thus triggering further melting; (2) hydration of young lithosphere by the subduction fluid followed by reheating by a propagating spreading centre; and (3) decompression melting of depleted and subsequently hydrated mantle as it is tapped by a spreading centre. In either case, however, the geochemical data from the subduction-enriched magmas is consistent with an origin of second-stage melts and formation of arc-like crust, and this may require generation from a relatively refractory source, most likely residual from previous MORB extraction, that was subsequently enriched in subduction-mobile LILE and LREE.

Geological evidence for similar SSZ-type extensional settings for many other ophiolite suites in

Anatolia, as well as in other parts of the eastern Mediterranean, suggests that this type of tectonic environment may have been a common characteristic of closure of the Tethyan domain in this region (e.g. Yalınız, Floyd & Göncüoğlu, 1996; Robertson, 2002; Hoeck *et al.* 2002; Bortolotti *et al.* 2002; Beccaluva *et al.* 2004; Parlak *et al.* 2004; Göncüoğlu, Yalınız & Tekin, 2006*a*). The geological events occurring during the formation and evolution of many presently active arc-basin systems, such as the Mariana Trough, Manus Basin, Lau Basin (western Pacific) and the East Scotia Sea (e.g. Taylor & Martinez, 2003; Pearce, 2003), may provide a possible analogue for the complexity of the tectonic setting and evolution of the Tethyan oceanic realm in this region of the eastern Mediterranean.

8. Concluding remarks

The geochemical characteristics of basaltic lavas from the Tethyan suture zone ophiolites in western Turkey allow them to be divided into three broad subdivisions: (1) the MORB-type rocks that range in composition from LREE-depleted (N-MORB) through transitional to LREE-enriched (E-MORB) types; (2) the OIB-type alkaline basaltic rocks that are characterized by significant enrichment in LILE, HFSE and L-MREE, and a slight depletion in HREE, relative to MORB compositions; and (3) the SSZ-type tholeiites originated from mantle sources that are characterized by selective enrichments in fluid-soluble large ion lithophile elements (LILE) and LREE relative to the high field strength elements (HFSE).

The geochemical characteristics and temporal distributions of the eruptive products suggest two distinct stages of melt production. The first of these stages is characterized by the formation of MORB–OIB-type eruptive rock associations and is considered to be related to the opening stage of an oceanic basin, while the second stage is marked by the formation of SSZ-type tholeiitic lavas. The modelling indicates that N-MORB, E-MORB and OIB compositions in the first stage are intimately linked in the melting process and that at least two compositionally distinct mantle sources, one similar to the depleted MORB mantle and the other more enriched than the depleted MORB mantle, play a role in producing these subduction-unmodified basaltic lavas. Among the subduction-unmodified basaltic lavas, the most depleted (N-MORB) and the most enriched (OIB) compositions can be interpreted to represent melting of the depleted and enriched components, respectively, and melting-induced mixing of multi-component mantle can be considered a viable mechanism to produce the MORB–OIB compositions.

The existence of SSZ-type tholeiites with geochemical signatures indicative of pre-melting subduction influence provides evidence for the development of arc-like crust by melting of a mantle source above a subduction zone. The relative depletion in HFSE and REE for some of the SSZ basalts with respect to the average N-MORB composition further suggests generation from a relatively refractory source, which was most likely experienced from previous melting and MORB extraction and subsequent enrichment in subduction-mobile elements. This second-stage melt generation is likely to be explained by development of an arc–back-arc system in proximity to an active spreading centre, during which the SSZ-type crust generation is related to initiation of intra-oceanic subduction within a pristine MORB lithosphere.

Acknowledgements. This study was carried out as part of a research project funded in part by the University of Kocaeli and TÜBİTAK (199Y100). Gurhan Baltic is thanked for his help with the sampling in the field. We would like to thank two anonymous referees for their constructive reviews and David Pyle for much helpful editorial handling.

References

ALDANMAZ, E. 2002. Mantle source characteristics of alkali basalts and basanites in an extensional intracontinental plate setting, western Anatolia, Turkey: Implications for multi-stage melting. *International Geology Review* **44**, 440–57.

ALDANMAZ, E., GOURGAUD, A. & KAYMAKCI, N. 2005. Constraints on the composition and thermal structure of the upper mantle beneath NW Turkey: evidence from mantle xenoliths and alkali primary melts. *Journal of Geodynamics* **39**, 277–316.

ALDANMAZ, E., KÖPRÜBAŞI, N., GÜRER, O. F., KAYMAKCI, N. & GOURGAUD, A. 2006. Geochemical constraints on the Cenozoic, OIB-type alkaline volcanic rocks of NW Turkey: Implications for mantle sources and melting processes. *Lithos* **86**, 50–76.

ALDANMAZ, E. & KÖPRÜBAŞI, N. 2006. Platinum-group element systematics of peridotites from ophiolite complexes of NW Anatolia, Turkey: Implications for mantle metasomatism by melt percolation in a supra-subduction zone environment. *International Geology Review* **48**, 420–42.

ALDANMAZ, E., PEARCE, J. A., THIRLWALL, M. F. & MITCHELL, J. G. 2000. Petrogenetic Evolution of Late Cenozoic, Post-Collision Volcanism in Western Anatolia, Turkey. *Journal of Volcanology and Geothermal Research* **102**, 67–95.

ALLÈGRE, C. J. & TURCOTTE, D. L. 1986. Implications of a two component marble-cake mantle. *Nature* **323**, 123–7.

BARRY, T. L., PEARCE, J. A., LEAT, P. T., MILLAR, I. L. & le ROEX, A. P. 2006. Hf isotope evidence for selective mobility of high-field-strength elements in a subduction setting: South Sandwich Islands. *Earth and Planetary Science Letters* **252**, 223–44.

BECCALUVA, L., COLTORTI, M., GIUNTA, G. & SIENA, F. 2004. Tethyan vs. Cordilleran ophiolites: A reappraisal of distinctive tectono-magmatic features of supra-subduction complexes in relation to the subduction mode. *Tectonophysics* **393**, 163–74.

BORTOLOTTI, V., MARRONI, M., PANDOLFI, L., PRINCIPI, G. & SACCANI, E. 2002. Interaction between mid-ocean ridge and subduction magmatism in Albanian ophiolites. *Journal of Geology* **110**, 561–76.

BOYNTON, W. V. 1984. Geochemistry of the rare earth elements: meteorite studies. In *Rare Earth Element Geochemistry* (ed. P. Henderson), pp. 63–114. Elsevier.

COUSENS, B. L., ALLAN, J. F., LEYBOURNE, M. I. & CHASE, R. L. 1995. Mixing of magmas from enriched and depleted mantle sources in the northeast Pacific–West Valley Segment, Juan de Fuca Ridge. *Contributions to Mineralogy and Petrology* **120**, 337–57.

DEBAILLE, V., BLICHERT-TOFT, J., AGRANIER, A., DOUCELANCE, R., SCHIANO, P. & ALBARÈDE, F. 2006. Geochemical component relationships in MORB from the Mid-Atlantic Ridge, 22–35°N. *Earth and Planetary Science Letters* **241**, 844–62.

DILEK, Y., THY, P., HACKER, B. & GRUNDVING, S. 1999. Structure and petrology of Tauride ophiolites and mafic dike intrusions (Turkey): implications for the Neotethyan ocean. *Geological Society of America Bulletin* **111**, 1192–1216.

DONNELLY, K. E., GOLDSTEIN, S. L., LANGMUIR, C. H. & SPIGELMAN, M. 2004. Origin of enriched ocean ridge basalts and implications for mantle dynamics. *Earth and Planetary Science Letters* **226**, 347–66.

DUPRE, B., LAMBERT, B., ROUSSEAU, D. & ALLÈGRE, C. J. 1981. Limitation on the scale of mantle heterogeneity under oceanic ridges. *Nature* **294**, 552–4.

ERDOĞAN, B. 1990. Tectonic relations between İzmir-Ankara zone and Karaburun belt. *Bulletin of the Mineral Research and Exploration (Foreign Edition)* **110**, 1–15.

GÖNCÜOĞLU, M. C., DIRIK, K. & KOZLU, H. 1997. General characteristics of pre-Alpine and Alpine terranes in Turkey: Explanatory notes to the terrane map of Turkey. *Annales Geologique de Pays Hellenique* **37**, 515–36.

GÖNCÜOĞLU, M. C., TURHAN, N., SENTURK, K., ÖZCAN, A. & UYSAL, S. 2000. A geotraverse across NW Turkey: tectonic units of the Central Sakarya region and their tectonic evolution. In *Tectonics and Magmatism in Turkey and the Surrounding Area* (eds E. Bozkurt, J. A. Winchester & J. D. A. Piper), pp. 139–61. Geological Society of London, Special Publication no. 173.

GÖNCÜOĞLU, M. C., YALINIZ, M. K. & TEKIN, U. K. 2006*a*. Geochemistry, tectono-magmatic discrimination and radiolarian ages of basic extrusives within the İzmir–Ankara suture belt (NW Turkey): time constraints for the neotethyan evolution. *Ofioliti* **31**, 25–38.

GÖNCÜOĞLU, M. C., YALINIZ, M. K. & TEKIN, U. K. 2006*b*. Geochemical features and radiolarian ages of volcanic rocks from the İzmir–Ankara suture belt, western Turkey. In *Proceedings of the International Symposium on Mesozoic Ophiolite Belts of Northern Part of the Balkan Peninsula, 11 May–6 June 2006 Banja Luka-Belgrade*, pp. 41–4.

GRAHAM, D. W., BLICHERT-TOFT, J., RUSSO, J. C., RUBIN, K. H. & ALBARÈDE, F. 2006. Cryptic striations in the upper mantle revealed by hafnium isotopes in southeast Indian ridge basalts. *Nature* **440**, 199–202.

GÜRER, O. F. & ALDANMAZ, E. 2002. Origin of the upper Cretaceous–Tertiary sedimentary basins within the Tauride–Anatolide platform in Turkey. *Geological Magazine* **139**, 191–7.

HAWKESWORTH, C. J., TURNER, S. P., MCDERMOTT, F., PEATE, D. W. & VAN CALSTEREN, P. 1997. U–Th isotopes in arc magmas: implications for element transfer from the subducted crust. *Science* **276**, 551–5.

HOECK, V., KOLLER, F., MEISEL, T., ONUZI, K. & KNERINGER, E. 2002. The Jurassic South Albanian ophiolites: MOR- vs. SSZ-type ophiolites. *Lithos* **65**, 143–64.

HOFMANN, A. W. 1997. Mantle geochemistry: the message from oceanic volcanism. *Nature* **385**, 219–29.

ITO, G., LIN, J. & GRAHAM, D. 2003. Observational and theoretical studies of the dynamics of mantle plume-mid ocean ridge interactions. *Reviews of Geophysics* **41**, article no: 1017, 24 pp., doi: 10.1029/2002RG000117.

KORENAGA, J. 2004. Mantle mixing and continental breakup magmatism. *Earth and Planetary Science Letters* **218**, 463–73.

LEAT, P. T., PEARCE, J. A., BARKER, P. F., MILLAR, I. L., BARRY, T. L. & LARTER, R. D. 2004. Magma genesis and mantle flow at a subducting slab edge: the South Sandwich arc-basin system. *Earth and Planetary Science Letters* **227**, 17–35.

LUNDSTROM, C. C., SAMPSON, D. E., PERFIT, M. R., GILL, J. & WILLIAMS, Q. 1999. Insights into mid-ocean ridge basalt petrogenesis: U-series disequilibria from the Siqueiros Transform, Lamont Seamounts, and East Pacific Rise. *Journal of Geophysical Research* **104**, 13034–48.

MCCULLOCH, M. T. & GAMBLE, J. A. 1991. Geochemical and geodynamical constraints on subduction zone magmatism. *Earth and Planetary Science Letters* **102**, 358–74.

MEIBOM, A. & ANDERSON, D. L. 2003. The statistical upper mantle assemblage. *Earth and Planetary Science Letters* **217**, 123–39.

MIYASHIRO, A. 1973. The Troodos ophiolitic complex was probably formed in an island arc. *Earth and Planetary Science Letters* **19**, 218–24.

NIU, Y., BIDAEU, D., HÈKINIAN, R. & BATIZA, R. 2001. Mantle compositional control on the extent of mantle melting, crust production, gravity anomaly, ridge morphology, and ridge segmentation: a case study at the mid-Atlantic ridge 33–35N. *Earth and Planetary Science Letters* **186**, 383–99.

NIU, Y., COLLERSON, K. D. & BATIZA, R. 1999. Origin of enriched-type mid-ocean ridge basalts at ridges far from mantle plumes: the East Pacific Rise at 1120′. *Journal of Geophysical Research* **104**, 7067–87.

NIU, Y., REGELOUS, M., WENDT, I. J., BATIZA, R. & O'HARA, M. J. 2002. Geochemistry of near-EPR seamounts: importance of source vs. process and the origin of enriched mantle component. *Earth and Planetary Science Letters* **199**, 327–41.

OKAY, A. I. 2002. Jadeite-chloritoid-lawsonite blueschists in northwest Turkey: unusually high P/T ratios in continental crust. *Journal of Metamorphic Geology* **20**, 757–68.

OKAY, A. I., TANSEL, I. & TÜYSÜZ, O. 2001. Obduction, subduction and collision as reflected in the Upper Crateceous–Lower Eocene sedimentary record of western Turkey. *Geological Magazine* **138**, 117–42.

ÖNEN, A. P. 2003. Neotethyan ophiolitic rocks of the Anatolides of NW Turkey and comparison with Tauride ophiolites. *Journal of the Geological Society, London* **160**, 947–62.

PARLAK, O., HOECK, V., KOZLU, H. & DELALOYE, M. 2004. Oceanic crust generation in an island arc tectonic setting, SE Anatolian orogenic belt (Turkey). *Geological Magazine* **141**, 583–603.

PEARCE, J. A. 2003. Supra-subduction zone ophiolites: The search for modern analogues. In *Ophiolite Concept and Evolution of Geological Thought* (eds Y. Dilek & S. Newcomb), pp. 269–93. Geological Society of America, Special Publication no. 373.

PEARCE, J. A. 2005. Mantle preconditioning by melt extraction during flow: theory and petrogenetic implications. *Journal of Petrology* **46**, 973–97.

PEARCE, J. A., BAKER, P. E., HARVEY, P. K. & LUFF, I. W. 1995. Geochemical evidence for subduction fluxes, mantle melting and fractional crystallization beneath the South Sandwich arc. *Journal of Petrology* **36**, 1073–1109.

PEARCE, J. A., KEMPTON, P. D., NOWELL, G. M. & NOBLE, S. R. 1999. Hf–Nd element and isotope perspective on the nature and provenance of mantle and subduction components in Western Pacific arc-basin systems. *Journal of Petrology* **40**, 1579–1611.

PEARCE, J. A. & NORRY, M. J. 1979. Petrogenetic Implications of Ti, Zr, Y and Nb variations in volcanic rocks. *Contributions to Mineralogy and Petrology* **69**, 33–47.

PEARCE, J. A. & PEATE, D. W. 1995. Tectonic implications of the composition of volcanic arc magmas. *Annual Review of Earth Planetary Sciences* **23**, 251–85.

PEARCE, J. A., STERN, R. J., BLOOMER, S. H. & FRYER, P. 2005. Geochemical mapping of the Mariana arc-basin system: implication for the nature and distribution of the subduction component. *Geochemistry Geophysics Geosystems* **6**, article no: Q07006, 27 pp., doi: 10.1029/2004GC000895.

ROBERTSON, A. H. F. 2002. Overview of the genesis and emplacement of Mesozoic ophiolites in the Eastern Mediterranean Tethyan region. *Lithos* **65**, 1–67.

SCHILLING, J. G. 1973. Iceland mantle plume: geochemical study of the Reykjanes Ridge. *Nature* **242**, 565–71.

ŞENGÖR, A. M. C. & YILMAZ, Y. 1981. Tethyan evolution of Turkey: A plate tectonic approach. *Tectonophysics* **75**, 181–241.

SHERLOCK, S., KELLEY, S., INGER, S., HARRIS, N. B. W. & OKAY, A. I. 1999. ^{40}Ar–^{39}Ar and Rb–Sr geochronology of high-pressure metamorphism and exhumation history of the Tavşanlı zone, NW Turkey. *Contributions to Mineralogy and Petrology* **137**, 46–58.

SHERVAIS, J. W. 2001. Birth, death, and resurrection: The life cycle of suprasubduction zone ophiolites. *Geochemistry Geophysics Geosystems* **2**, article no: GC000080, 45 pp., doi: 10.1029/2000GC000080.

SLATER, L., MCKENZIE, D., GRONVOLD, K. & SHIMIZU, N. 2001. Melt generation and movement beneath Theistareykir, NE Iceland. *Journal of Petrology* **42**, 321–54.

SLEEP, N. H. 1984. Tapping of magmas from ubiquitous mantle heterogeneities: an alternative to mantle plumes? *Journal of Geophysical Research* **89**, 10029–41.

SUN, S.-S. & MCDONOUGH, W. F. 1989. Chemical and isotopic systematics of oceanic basalts: implications for mantle composition and processes. In *Magmatism in the Ocean Basins* (eds A. D. Saunders & M. J. Norry), pp. 313–45. Geological Society of London, Special Publication no. 42.

TAYLOR, B. & MARTINEZ, F. 2003. Back-arc basin basalt systematics. *Earth and Planetary Science Letters* **210**, 481–97.

TEKIN, U. K., GÖNCÜOĞLU, M. C. & TURHAN, N. 2002. First evidence of Late Carnian radiolarian fauna from the İzmir–Ankara suture complex, Central Sakarya, Turkey: Implications for the opening age of the İzmir–Ankara branch of Neotethys. *Geobios* **35**, 127–35.

THIRLWALL, M. F., SMITH, T. E., GRAHAM, A. M., THEODOROU, N., HOLLINGS, P., DAVIDSON, J. P. & ARCULUS, R. J. 1994. High Field Strength Element Anomalies in Arc Lavas: Source or Process? *Journal of Petrology* **35**, 819–38.

WOOD, D. A. 1980. The application of a Th–Hf–Ta diagram to problems of tectonomagmatic classification and to establishing the nature of crustal contamination of basaltic lavas of the British tertiary volcanic province. *Earth and Planetary Science Letters* **50**, 11–30.

WOODHEAD, J., EGGINS, S. & GAMBLE, J. 1993. High field strength and transition element systematics in island arc and back-arc basalts: evidence for multi-phase melt extraction and a depleted mantle wedge. *Earth and Planetary Science Letters* **114**, 491–504.

YALINIZ, M. K., FLOYD, P. A. & GÖNCÜOĞLU, M. C. 1996. Supra-subduction zone ophiolites of Central Anatolia: Geochemical evidence from the Sarikaraman ophiolite, Aksaray, Turkey. *Mineralogical Magazine* **60**, 697–710.